

**SENSITIVITY AND SPECIFICITY OF THE
MULTI-CHANNEL CW-fNIRS FOR MEDICAL PURPOSES**

by

Alp Özdemir

B.S., Electrical & Electronics Engineering, Boğaziçi University, 2011

Submitted to the Institute of Biomedical Engineering

in partial fulfillment of the requirements

for the degree of

Master of Science

in

Biomedical Engineering

Boğaziçi University

2013

ACKNOWLEDGMENTS

There are a number of people without whom this thesis might not have been written.

First and foremost, I would like to express my deepest gratitude to my supervisor Assoc.Prof.Dr. Ata Akın for his invaluable guidance and advice. His willingness to motivate me contributed tremendously to this study. I thank my thesis readers Prof. Dr. Ahmet Ademođlu and Assist.Prof.Dr. Yasemin Keskin Ergen for their valuable feedback.

I am sure that spending 3 years in NOILab have made me a better academic and have also included a lot of lovely people to my life. I owe many thanks to all of them. I would like to thank especially to Pınar Adanalı and Sinem Burcu Erdoğan for their kind friendship and big effort to keep my motivation high. Thanks a lot to Mehmet Ufuk Dalmıř and Seda Dumlu for their precious suggestions on my study.

My dearest friends, Mert Yılmaz, Mehmet Avcı, Celal Kopuz and GÜNCE Eseryel have been always with me for years and I could not slight their support on me.

Many thanks to my family for their constant love and endless support throughout my life.

Finally, I would like to thank Bige Vardar to make my life more colorful in this period.

Although I will be a little bit away from here for a while, my heart will always with you. Thank you all...

ABSTRACT

SENSITIVITY AND SPECIFICITY OF THE MULTI-CHANNEL CW-fNIRS FOR MEDICAL PURPOSES

In last decades, optical imaging technology has been rapidly developed and become much popular for scientific researches. Its safe, non-invasive and portable design easily integrates fNIRS to different research areas and makes it much preferable especially for brain researchers. Since fNIRS sensitively scan neurobiological changes in the PFC during neurological and psychiatric disorders, many studies benefits from the convenience of fNIRS to extend the understanding about these disorders. This study aims to present reflections of different PFC related disorders which are schizophrenia, migraine and attention deficit & hyperactivity disorder (ADHD) on fNIRS measurements and to reveal their differences from control group via advanced signal processing application. For this purpose, collected fNIRS measurements during cognitive task were preprocessed to remove artifacts and prepared for further analysis. Pre-processed signal sets were used to create feature set for each subject with the assistance of independent component analysis. Then these feature sets were investigated by clustering algorithm to observe discrimination of experimental groups and performance of the system was reported. In some cases, proposed system presents success rates up to 82% for migraine group, 92% for schizophrenia group and 95% ADHD group.

Keywords: fNIRS, Signal Processing, Schizophrenia, Migraine, Attention Deficit & Hyperactivity Disorder, Independent Component Analysis ,Clustering

ÖZET

ÇOK KANALLI SD-iYKAS SİSTEMİNİN MEDİKAL AMAÇLI HASSASİYETİ VE ÖZGÜLLÜĞÜ

Optik görüntüleme teknolojisinin son yıllarda gösterdiği hızlı gelişmeler, bu teknolojiyle yapılan bilimsel çalışmaların popülaritesini artırmıştır. Güvenli, portatif ve non-invasif tasarımı, iYKAS'ın başta beyin araştırmaları olmak üzere birçok farklı bilimsel alanda kullanımını yaygınlaştırmıştır. iYKAS teknolojisinin nörolojik veya psikolojik rahatsızlıklar esnasında dahi hassas bir şekilde prefrontal kortexteki nörobiyolojik olayları ölçümleyebiliyor olması, bu hastalıkların araştırılmasında daha sık tercih edilmesine sebep olmaktadır. Bu çalışma, prefrontal kortekste etkilerini gösteren migren, şizofreni ve ADHD (dikkat eksikliği ve hiperaktivite bozukluğu) rahatsızlıklarının iYKAS ölçümleri üzerindeki yansımalarını göstermeyi ve ileri seviyede sinyal işleme teknikleriyle sağlıklı deneklerle olan farklılıklarını ortaya koymayı amaçlamıştır. Bu sebeple, deneklere uygulanan bilişsel görevler esnasında toplanan iYKAS ölçümleri önışlemeden geçirilip artefaktlardan temizlenip daha sonraki analiz için hazırlanmıştır. Her bir denekten toplanmış olup önışlemeden geçirilen bu sinyaller bağımsız bileşenler analizi yardımıyla özellik seti oluşturmada kullanılmıştır. Oluşturulan özellik setleri kümeleme algoritması yardımıyla incelenmiş, deney grupları arasındaki farklılıklar ortaya konulmuş ve kurulan sistemin performansı raporlanmıştır. Önerilen sistem migren grubu için %82'ye, şizofren grubu için %92'ye ve ADHD grubu için %95'e ulaşan doğrulukta sonuçlar vermiştir.

Anahtar Sözcükler: Yakın Kızılaltı Spektroskopi, Sinyal İşleme, Şizofreni, Migren, Dikkat Eksikliği ve Hiperaktivite Bozukluğu, Bağımsız Bileşenler Analizi, Kümeleme

TABLE OF CONTENTS

ACKNOWLEDGMENTS	iii
ABSTRACT	iv
ÖZET	v
LIST OF FIGURES	viii
LIST OF TABLES	xi
LIST OF ABBREVIATIONS	xii
1. INTRODUCTION	1
2. PRINCIPLES OF NEURO-OPTICAL IMAGING	3
2.1 functional Near Infrared Spectroscopy	3
2.2 Experimental Groups & Applied Task	5
3. METHODOLOGY	7
3.1 Pre-processing	7
3.1.1 Band-pass Filtering	8
3.1.2 Artifact Removal by Modified PCA Algorithm	8
3.1.3 Noisy Channel Decision	12
3.2 Feature Extraction	12
3.2.1 Feature Extraction from ICA Output	13
3.3 Clustering	16
4. RESULTS	17
4.1 Results for Control vs. Migraine Groups	18
4.2 Results for Control vs. Schizophrenia Groups	21
4.3 Results for Control vs. ADHD Groups	24
4.4 Results for Schizophrenia vs. Migraine Groups	27
4.5 Results for ADHD vs. Migraine Groups	30
4.6 Results for ADHD vs. Schizophrenia Groups	33
4.7 Results for Discrimination of All Groups Together	36
5. DISCUSSIONS	40
6. CONCLUSIONS	42
APPENDIX A. Independent Component Analysis	44

APPENDIX B. Feature Selection Algorithm	46
APPENDIX C. Fuzzy C-Means Clustering	47
APPENDIX D. Additional Figures for Results	49
REFERENCES	74

LIST OF FIGURES

Figure 2.1	Illustration of 16-channel fNIRS probe	5
Figure 2.2	Example for neutral, congruent and incongruent questions of color-word matching Stroop test [1].	6
Figure 3.1	Flowchart of the proposed system	7
Figure 3.2	Flowchart of the preprocessing step	8
Figure 3.3	A typical baseline drift observed at the HbO ₂ signal is removed by 4th order 0.01-0.8 Hz Butterworth filter from the Xth channel of a subject. Red line is the filtered data.	8
Figure 3.4	Sample for principal component and corresponding moving standard deviation function	10
Figure 3.5	Samples for output (blue line) of artifact removal algorithm.	11
Figure 3.6	Sample for discarded measurements from the analysis	12
Figure 3.7	Sample for independent components which are dominant at different frequency range. (a) Component on left is more dominant at 0.4-0.5Hz and 0.5-0.6Hz intervals while the one at the right (b) is more dominant at 0-0.1 and 0.1-0.2Hz.	15
Figure 4.1	Channel distribution (a) and frequency band distribution (b) of selected <i>HbO₂</i> features for Control-Migraine discrimination	19
Figure 4.2	True map (a) and clustering result (b) based on selected <i>HbO₂</i> features for Control-Migraine discrimination	20
Figure 4.3	Channel distribution (a) and frequency band distribution (b) of selected <i>HbT</i> features for Control-Schizophrenia discrimination	22
Figure 4.4	True map (a) and clustering result (b) based on selected <i>HbT</i> features for Control-Schizophrenia discrimination	23
Figure 4.5	Channel distribution (a) and frequency band distribution (b) of selected <i>HbT</i> features for Control-ADHD discrimination	25
Figure 4.6	True map (a) and clustering result (b) based on selected <i>HbT</i> features for Control-ADHD discrimination	26

Figure 4.7	Channel distribution (a) and frequency band distribution (b) of selected HbO_2 features for Schizophrenia & Migraine discrimination	28
Figure 4.8	True map (a) and clustering result (b) based on selected HbO_2 features for Schizophrenia & Migraine discrimination	29
Figure 4.9	Channel distribution (a) and frequency band distribution (b) of selected HbO_2 features for ADHD-Migraine discrimination	31
Figure 4.10	True map (a) and clustering result (b) based on selected HbO_2 features for ADHD-Migraine discrimination	32
Figure 4.11	Channel distribution (a) and frequency band distribution (b) of selected HbT features for ADHD-Schizophrenia discrimination	34
Figure 4.12	True map (a) and clustering result (b) based on selected HbT features for ADHD-Schizophrenia discrimination	35
Figure 4.13	Channel distribution (a) and frequency band distribution (b) of selected Hb features for discrimination of all groups	38
Figure 4.14	True map (a) and clustering result (b) based on selected Hb features for discrimination of all groups	39
Figure D.1	Channel distribution (a) and frequency band distribution (b) of selected Hb features for Control-Migraine discrimination	50
Figure D.2	True map (a) and clustering result (b) based on selected Hb features for Control-Migraine discrimination	51
Figure D.3	Channel distribution (a) and frequency band distribution (b) of selected HbT features for Control-Migraine discrimination	52
Figure D.4	True map (a) and clustering result (b) based on selected HbT features for Control-Migraine discrimination	53
Figure D.5	Channel distribution (a) and frequency band distribution (b) of selected HbO_2 features for Control-Schizophrenia discrimination	54
Figure D.6	True map (a) and clustering result (b) based on selected HbO_2 features for Control-Schizophrenia discrimination	55
Figure D.7	Channel distribution (a) and frequency band distribution (b) of selected Hb features for Control-Schizophrenia discrimination	56
Figure D.8	True map (a) and clustering result (b) based on selected Hb features for Control-Schizophrenia discrimination	57

Figure D.9	Channel distribution (a) and frequency band distribution (b) of selected HbO_2 features for Control-ADHD discrimination	58
Figure D.10	True map (a) and clustering result (b) based on selected HbO_2 features for Control-ADHD discrimination	59
Figure D.11	Channel distribution (a) and frequency band distribution (b) of selected HbT features for Schizophrenia & Migraine discrimination	60
Figure D.12	True map (a) and clustering result (b) based on selected HbT features for Schizophrenia & Migraine discrimination	61
Figure D.13	Channel distribution (a) and frequency band distribution (b) of selected Hb features for ADHD-Migraine discrimination	62
Figure D.14	True map (a) and clustering result (b) based on selected Hb features for ADHD-Migraine discrimination	63
Figure D.15	Channel distribution (a) and frequency band distribution (b) of selected HbT features for ADHD-Migraine discrimination	64
Figure D.16	True map (a) and clustering result (b) based on selected HbT features for ADHD-Migraine discrimination	65
Figure D.17	Channel distribution (a) and frequency band distribution (b) of selected HbO_2 features for ADHD-Schizophrenia discrimination	66
Figure D.18	True map (a) and clustering result (b) based on selected HbO_2 features for ADHD-Schizophrenia discrimination	67
Figure D.19	Channel distribution (a) and frequency band distribution (b) of selected Hb features for ADHD-Schizophrenia discrimination	68
Figure D.20	True map (a) and clustering result (b) based on selected Hb features for ADHD-Schizophrenia discrimination	69
Figure D.21	Channel distribution (a) and frequency band distribution (b) of selected HbO_2 features for discrimination of all groups	70
Figure D.22	True map (a) and clustering result (b) based on selected HbO_2 features for discrimination of all groups	71
Figure D.23	Channel distribution (a) and frequency band distribution (b) of selected HbT features for discrimination of all groups	72
Figure D.24	True map (a) and clustering result (b) based on selected HbT features for discrimination of all groups	73

LIST OF TABLES

Table 3.1	Frequency intervals of the specified bands	14
Table 4.1	Illustration of True/False and Positive/Negative terms	18
Table 4.2	Clustering indexes for control & migraine groups	18
Table 4.3	Clustering indexes for control & schizophrenia groups	21
Table 4.4	Clustering indexes for control & ADHD groups	24
Table 4.5	Clustering indexes for Schizophrenia & Migraine Groups	27
Table 4.6	Clustering indexes for ADHD & migraine groups	30
Table 4.7	Clustering indexes for ADHD & schizophrenia groups	33
Table 4.8	Clustering results of selected HbO_2 features for all experimental groups together	36
Table 4.9	Clustering results of selected Hb features for all experimental groups together	37
Table 4.10	Clustering results of selected HbT features for all experimental groups together	37

LIST OF ABBREVIATIONS

<i>fNIRS</i>	Functional Near-Infrared Spectroscopy
<i>Hb</i>	Deoxy-hemoglobin
<i>HbO₂</i>	Oxy-hemoglobin
<i>HbT</i>	Total-hemoglobin
<i>PFC</i>	Pre-Frontal Cortex
<i>PCA</i>	Principal Component Analysis
<i>ICA</i>	Independent Component Analysis
<i>MSD</i>	Moving Standard Deviation
<i>FDR</i>	Fisher's Discrimination Ratio
<i>FCM</i>	Fuzzy C-Means
<i>fMRI</i>	Functional Magnetic Resonance Imaging
<i>PET</i>	Positron Emission Tomography
<i>ADHD</i>	Attention Deficit & Hyperactivity Disorder

1. INTRODUCTION

Cognitive neuroscience has been in search of systems that would enable researchers to explain the behavioral differences with respect to neurobiological changes. In many pathological cases (i.e. psychiatric and neurological disorders) the abnormalities observed in the behavior have strong correlations with the impairments in respective neurobiology. In most cases these impairments can only be found via invasive (i.e. PET scans) or very expensive techniques (i.e. fMRI scans). Hence there has been a trend to develop rapid, non-invasive and accurate biomedical systems to determine the link between the behavior and biology and use these systems in clinical settings for improved diagnostic and therapeutic protocols. The functional near-infrared spectroscopy (fNIRS) developed at the Neuro-Optical Imaging laboratory over the last 8 years is a proposed system to address these issues.

fNIRS is an optical neuro-imaging method for measuring the hemodynamic responses in response to neuronal activation in the prefrontal cortex of the brain that is based on the hypothesis of neuro-vascular coupling. The technique depends on placing a probe housing light sources and detectors on the subject's forehead and connecting it to a data acquisition box and then a computer. The data is recorded and then analyzed for changes in the blood flow or its oxygenation levels of the brain.[2, 3]

One of the promises of fNIRS has been the rapid and easy scanning of the neurobiological changes in the PFC during neurological and psychiatric disorders. There have been many studies to assess the feasibility to use fNIRS in these disorders [4, 5, 6, 7, 8, 9, 10, 11, 12]. In most cases the power of fNIRS as a diagnostic tool has been investigated for a specific type of disease (i.e. migraine, schizophrenia, attention deficit and hyperactivity disorder, etc). These diseases are all PFC related diseases and they exhibit themselves as an impairment in executive functions.

Migraine is proposed to be a neurovascular coupling disorder where the neuronal activity-induced metabolic demand, such as oxygen or glucose, is not provided by the vascular supply. It was suggested that patients with migraine may present altered values of the parameters related to their cerebral circulation. Even during the interictal period several studies reported hypoperfusion, decrease in the regional cerebral blood flow, and changes in the cerebrovascular reactivity [10, 9, 13, 14, 15, 8, 16, 7].

Schizophrenia is a psychiatric disorder and prefrontal cortex dysfunction has been shown as one of the characteristic of the disease [11, 17, 18]. This absence of adequate functionality on prefrontal area of the cerebral cortex also affects the performance of the patients during cognitive tasks and results in successfully differentiate these patients from healthy subjects [19, 5, 20].

Attention deficit/hyperactivity disorder is a disorder related with central nervous system and can be seen in both childhood and adulthood [21]. It has been reported that ADHD patients shows poor performance across frontal lobe tests. fNIRS is one of the useful modality to observe hemodynamic changes on prefrontal cortex and is also preferred in ADHD studies [6, 22, 23, 4].

In this project, clinical data previously collected by the 16 channel fNIRS system developed at the Neuro-Optical Imaging Laboratory will be analyzed and differences between patients and healthy controls will be investigated. Specifically I will attempt to develop novel signal processing techniques to quantify the sensitivity and specificity of this instrument for different illnesses (migraine, schizophrenia, attention deficit and hyperactivity disorder). Although there is not enough findings between these groups for fNIRS technology, similar studies for other imaging modalities motivates us for the possible results [24, 25, 26, 27].

2. PRINCIPLES OF NEURO-OPTICAL IMAGING

2.1 functional Near Infrared Spectroscopy

In the last decades, functional near-infrared spectroscopy (fNIRS) has taken a place as a new neuroimaging modality. Its portable, safe and noninvasive design attracts brain researchers to prefer this technology in their studies. fNIRS technology uses specific wavelengths of lights that can pass through the scalp and make it possible to measure relative oxygenated and deoxygenated hemoglobin concentration changes during cognitive or emotional brain activity [2, 3].

Optical imaging technology is based on measuring the attenuation of light as it passes through the underlying tissues. In brain imaging studies, changes in the attenuation means changes of HbO_2 and Hb concentrations in the underlying tissues which in turn represents the neural correlates of a specific cognitive activity at that specific area. This relationship is also known as theneurovascular coupling mechanism which relates functional neuronal brain activity to local hemodynamic changes.

In order to compute the concentration information of HbO_2 and Hb , it is required to convert light information obtained from measurements of optical attenuation at suitable wavelengths. It is known that the range of 710nm and 1000nm is the most useful interval to observe tissue oxygenation and using two light sources with different wavelengths one can extract relative information about HbO_2 and Hb concentration variation [28]. Change in optical density is measured as in equation 2.1 which is derived from Beer-Lambert Law. According to this, change in optical density at the specific wavelength (ΔOD^{λ_i}) depends on absorption coefficient of HbO_2 and Hb at this wavelength ($\epsilon_{HB,HBO_2}^{\lambda_i}$), concentration change of HbO_2 and Hb ($\Delta C_{HB,HBO_2}$) and source-detector distance (L).

$$\Delta OD^{\lambda_i} = \ln \left\{ \frac{I_0}{I} \right\} = \varepsilon_{HB, HbO_2}^{\lambda_i} \Delta C_{HB, HbO_2} L \quad (2.1)$$

Optical density information for two light source with different wavelengths is then converted to concentration change of HbO_2 and Hb information by using equations 2.2 and 2.3 [29, 30].

$$\Delta[HB] = \frac{\varepsilon_{HbO_2}^{\lambda_2} \Delta OD^{\lambda_1} - \varepsilon_{HbO_2}^{\lambda_1} \Delta OD^{\lambda_2}}{(\varepsilon_{HB}^{\lambda_1} \varepsilon_{HbO_2}^{\lambda_2} - \varepsilon_{HB}^{\lambda_2} \varepsilon_{HbO_2}^{\lambda_1}) L} \quad (2.2)$$

$$\Delta[HbO_2] = \frac{\varepsilon_{HB}^{\lambda_1} \Delta OD^{\lambda_2} - \varepsilon_{HB}^{\lambda_2} \Delta OD^{\lambda_1}}{(\varepsilon_{HB}^{\lambda_1} \varepsilon_{HbO_2}^{\lambda_2} - \varepsilon_{HB}^{\lambda_2} \varepsilon_{HbO_2}^{\lambda_1}) L} \quad (2.3)$$

NIRS equipment which used in this study was developed in the Neuro-Optical Imaging Laboratory of the Institute of Biomedical Engineering, Bogazici University. Illustration of prefrontal cortex probe of the system can be seen in figure 2.1. Probe has four light source and ten optical sensors and they placed in rectangular probe with 2.5 cm source-sensor space. This design allows 16 photon paths which means 16 different location for taking measurements from prefrontal cortex. The device uses LEDs which produce light with wavelength of 730nm and 850nm to obtain cerebral HbO_2 and Hb concentration information. Additionally, sampling frequency of the device is 1.6Hz which enables us to see response up to 0.8Hz according to Nyquist Theorem.

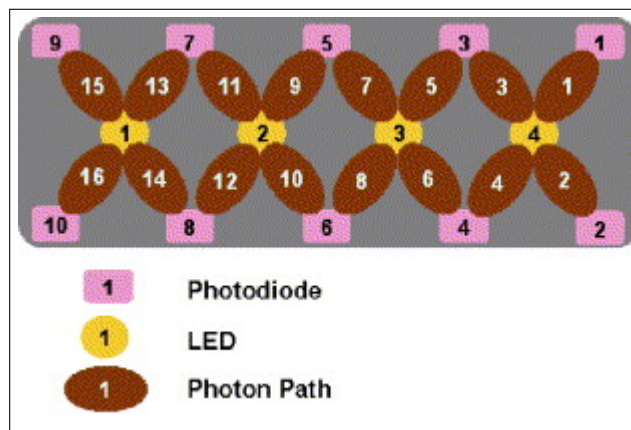


Figure 2.1 Illustration of 16-channel fNIRS probe

2.2 Experimental Groups & Applied Task

In this study, fNIRS measurements collected from a group of people during cognitive Stroop task were examined. Experimental group consist of 13 healthy adult controls, 15 adult migraine, 26 adult schizophrenia and 9 adult ADHD patients.

In order to see hemodynamic response of subjects, a cognitive task is applied during the measurement. For this reason, a modified version of the color-word matching Stroop task was used in the study [1]. Subjects were presented with two words, one written above the other. The upper word was written in different ink colors whereas the bottom one was in white over a black background. Subjects were asked to decide whether the word written below correctly denotes the color of the upper word or not. If the printed color of the upper word matches with the color name below, then subjects were to press on the left mouse button with their right index finger, and if not, on the right mouse button with their middle finger. This task consists of three different stimulus conditions as neutral, congruent and incongruent. In the neutral trials, upper word consisted of four X's (XXXX) printed in red, green, blue, or yellow. In the congruent trials ink color of the upper word and the word itself were the same, whereas in the incongruent condition, they were different. The trials were presented in a blocked manner. Each block consisted of six trials and there were 5 blocks for each condition. Inter-stimulus interval within the block was 4.5 s and the blocks were separated with 20 s interval during which the screen was blank. Subjects were informed to perform

the task as quickly and correctly as possible. The words stayed on the screen until the response was given with a maximum time of 3 s.

neutral	congruent	incongruent
XXXX BLUE	RED BLUE	GREEN BLUE
XXXX BLUE	BLUE BLUE	GREEN BLUE

Figure 2.2 Example for neutral, congruent and incongruent questions of color-word matching Stroop test [1].

3. METHODOLOGY

In this study, I attempt to evaluate fNIRS measurements to highlight the hemodynamic differences between the groups of patients who are schizophrenia, ADHD, migraine and healthy controls. To this aim, an algorithmic approach which consists of three main blocks (Figure 3.1) was developed. Firstly, preprocessing step was applied to fNIRS signals to reduce possible unfavorable effects of artifacts and noise on the measurements. Then, these processed signals were used to create a feature vector for each subject. These features were evaluated in clustering step and finally, performance of the system for all Hb, HbO₂ and HbT signals were observed separately.

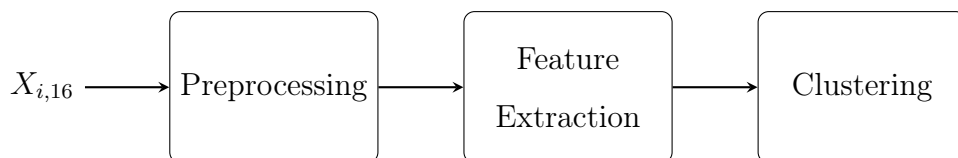


Figure 3.1 Flowchart of the proposed system

3.1 Pre-processing

Removing artifacts from physiological signals is an essential part of bio-signal processing studies and its robustness on the selectivity characteristic is the main factor which affects whole processing system. Artifacts on the fNIRS signals may result from various reasons such as imaging systems, environmental conditions or subject-specific conditions. Artifacts in fNIRS measurements are mainly due to subject-specific conditions because, other physiological signals may interfere to measurements and they may not be detected and removed totally. These artifacts are generally observed as drifts, spikes or jumps on the measurements. Preprocessing step of the system includes three sub-steps as seen in Figure 3.2.

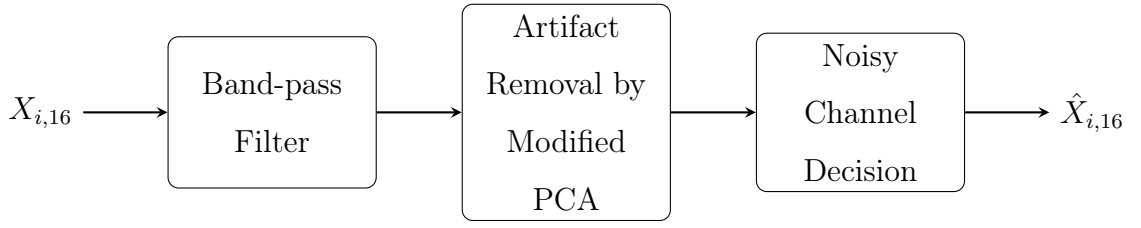


Figure 3.2 Flowchart of the preprocessing step

3.1.1 Band-pass Filtering

As a first step of preprocessing part of the analysis, in order to remove baseline drifts on measurements, Hb, HbO₂ and HbT signals were band-pass filtered by using 4th order Butter-worth filter in the frequency range of 0.01-0.8Hz (see Figure 3.3). By removing drift on the data, it is aimed to prevent from any negative effects like bias on the results.

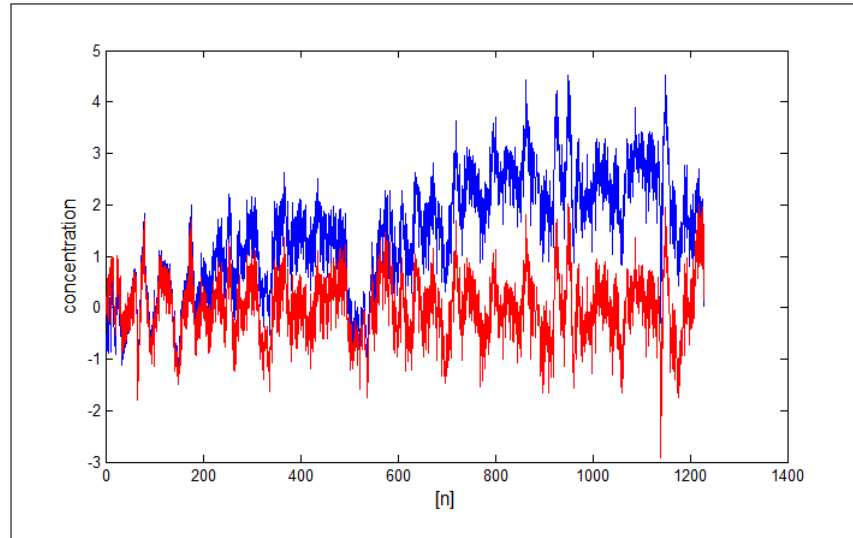


Figure 3.3 A typical baseline drift observed at the HbO₂ signal is removed by 4th order 0.01-0.8 Hz Butterworth filter from the Xth channel of a subject. Red line is the filtered data.

3.1.2 Artifact Removal by Modified PCA Algorithm

There are a lot of filtering techniques which are generally based on statistical estimation such as adaptive filtering and Kalman filtering. Statistical analysis methods like principal component analysis (PCA) and independent component analysis (ICA)

are also used effectively to remove artifacts from fNIRS signals [31] [32] [33] [34] [35]. PCA can be considered as a kind of transformation which represent the data in an orthogonal space that depends on maximum variance and it is commonly used to reduce dimensionality of datasets. Its performance of removing artefacts especially from fNIRS measurements has been shown in literature [31] [32] [34]. Because of its unsupervised structure, data will not be affected by model signal which mathematically represents embedded physiological signals or any similar outside information during the processing.

PCA assumes that signal set X_k is composed from n uncorrelated components Y_k and X_k can be interpreted as linear combination of Y_k 's.

$$X = \begin{pmatrix} x_1 \\ x_2 \\ \vdots \\ x_n \end{pmatrix} = WY = \begin{pmatrix} w_1 & w_2 & \cdots & w_n \end{pmatrix} \begin{pmatrix} y_1 \\ y_2 \\ \vdots \\ y_n \end{pmatrix}, \quad (3.1)$$

where X and Y contains the signals x_k and y_k , and W is the mixing matrix which contains eigenvectors of covariance matrix of X .

It was shown that removing principal components which have high eigen-values leads to a reduction of artifacts on measurements, since dominant characteristics of signal sets appears on those principal components [31] [32] [34]. However, removing whole component from the dataset also leads to some information loss. For this reason, detecting corrupted region on principal components and trying to clean out determined parts of signal sets will prevent from possible information loss. To this aim, computing moving standard deviation (Eqn 3.2) assists to specify corrupted regions [35]. Based on the information which comes from MSD functions, corrupted regions of principal components is removed while reconstructing signal-set from eigen-vectors and corre-

sponding coefficients.

$$s(t) = \frac{1}{2k+1} \left[\sum_{j=-k}^k x^2(t+j) - \frac{1}{2k+1} \left(\sum_{j=-k}^k x(t+j) \right)^2 \right]^{1/2} \quad (3.2)$$

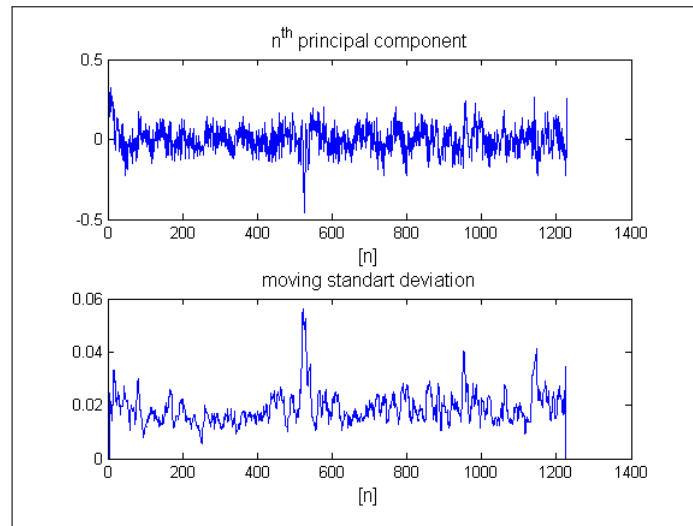


Figure 3.4 Sample for principal component and corresponding moving standart deviation function

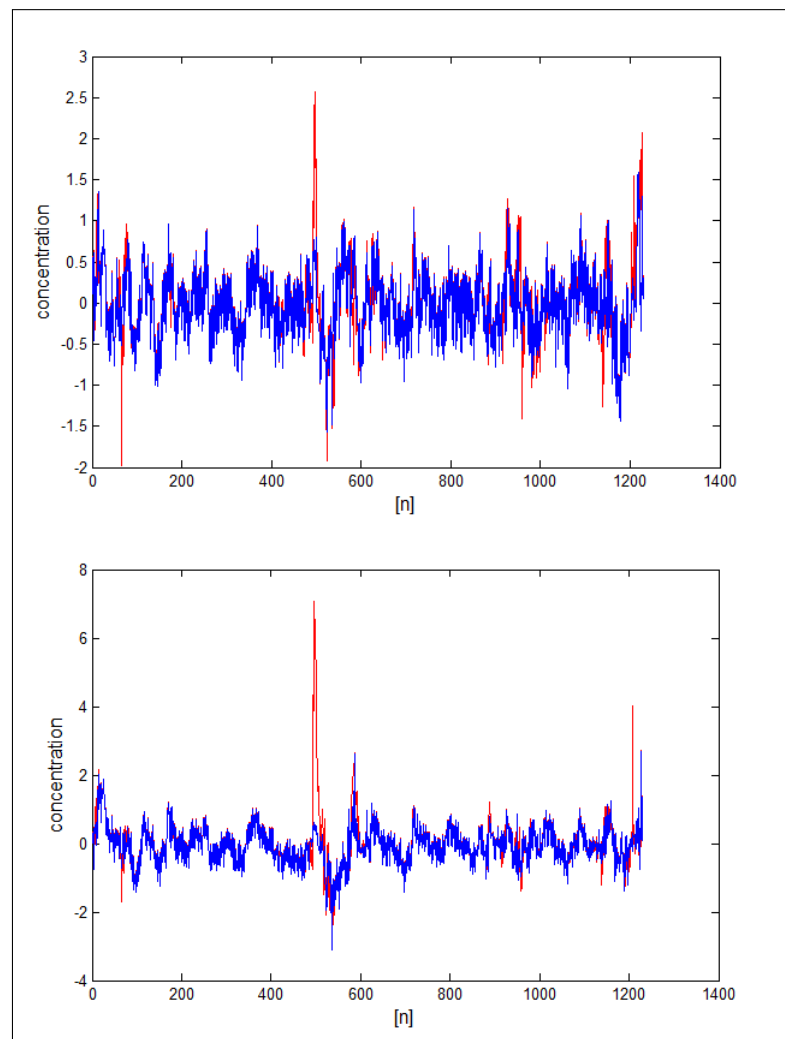


Figure 3.5 Samples for output (blue line) of artifact removal algorithm.

3.1.3 Noisy Channel Decision

Based on the visual inspection of the time course and spectral properties of the measurements, some of the channels were discarded from the analysis. Signals with relatively high variance and/or frequency characteristic corresponding to white noise were also excluded from the analysis (Figure 3.6).

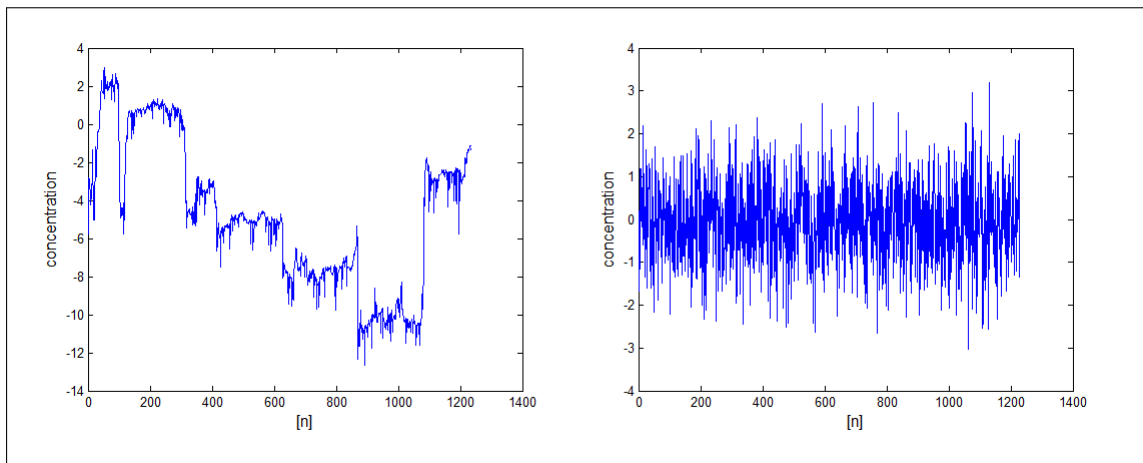


Figure 3.6 Sample for discarded measurements from the analysis

3.2 Feature Extraction

Different cerebral illnesses may show themselves by changing patterns in different imaging modalities [24, 25, 26, 27]. Methods like PCA and ICA which expose intrinsic information of multivariate signal sets are successfully used for finding these patterns. Especially studies which use ICA outputs in machine learning algorithms has been seen quite successful [25]. For this reason, it was decided to use ICA to extract features from fNIRS measurements and Fastica algorithm [36] was used to find the space axes which are maximally independent from each other. Fastica uses high order statistics to derive independent components from the negentropy information of data and it assumes that data includes nongaussian sources.

3.2.1 Feature Extraction from ICA Output

ICA is a method to extract subcomponents from the system of multivariate signals. Simply, ICA exposes hidden factors S from blended outputs X by assuming statistical independency and non-gaussianity of the factors. FastICA algorithm developed by Hyvarinen and Oja [36] (see Appendix A) was used to estimate the independent components, mixing A and the separation matrices W for each subject.

$$X = AS \tag{3.3}$$

$$\tilde{S} = WX \tag{3.4}$$

ICA decomposition was applied to expose dominant signals in the Hb, HbO2 and HbT signals. For each subject, spatially independent components were obtained with their corresponding weights given in the mixing matrix A .

The components and their weights extracted by ICA algorithm from each subject are used to create a feature set for clustering step. To this aim, frequency spectrum of each independent component was computed via fourier transform (Eqn 3.5) and these components were ranked based on the dominance of a specified frequency band as seen in Table 3.1. Dominance of these components was determined by calculating the power of the spectra within that specific frequency band (Eqn 3.6).

$$X_k = \sum_{n=0}^{N-1} x_n e^{-i2\pi k \frac{n}{N}} \tag{3.5}$$

$$Power = \int_{f_{lower}}^{f_{upper}} |X(f)| df \quad (3.6)$$

Table 3.1
Frequency intervals of the specified bands

Band	Interval
B1	0.01 - 0.1 Hz
B2	0.1 - 0.2 Hz
B3	0.2 - 0.3 Hz
B4	0.3 - 0.4 Hz
B5	0.4 - 0.5 Hz
B6	0.5 - 0.6 Hz
B7	0.6 - 0.7 Hz

For each subject, hemodynamic feature-set was created by using weights of the highest ranked independent components on specified frequency band. For each measurement channel, weights of top-ranked IC's, which are elements of the mixing matrix A (Eqn 3.3), are stored in feature-matrix. Since there are 7 frequency bands and 16 measurement channels, size of the feature-matrix of each subject becomes 7x16. Then, significant features on the feature matrix are determined by computing their score on Fisher's Discrimination Ratio (Eqn 3.7) and applying threshold.

$$FDR = \sum_{i=1}^n \sum_{j=1}^n \frac{(\mu_i - \mu_j)^2}{\sigma_i^2 + \sigma_j^2}, \quad (3.7)$$

where μ_i and σ_i are mean and variance of the feature for i^{th} group.

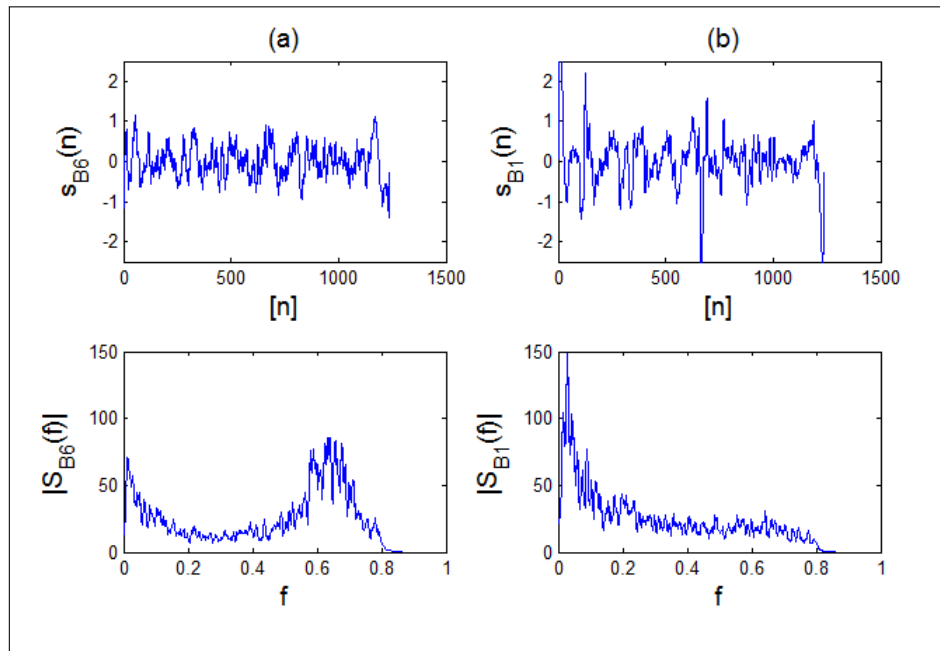


Figure 3.7 Sample for independent components which are dominant at different frequency range. (a) Component on left is more dominant at 0.4-0.5Hz and 0.5-0.6Hz intervals while the one at the right (b) is more dominant at 0-0.1 and 0.1-0.2Hz.

3.3 Clustering

Final step of this study is to investigate the discrimination ability of selected features. There are a lot of clustering and classification algorithms to check this ability. Since sizes of experimental groups are small and unequal, observing their clustering ability is much suitable than applying classification. Clustering results may also give good inspiration for further research to form much proper database.

K-means is well-known algorithm which is commonly used to cluster datasets, however its strict format and dependency to seeds as start points sometimes lead to show poor performance. If characteristics of the datasets are not known well, soft clustering algorithms like Fuzzy C-means have been seen much suitable. In literature, performance of the FCM and K-Means algorithms were compared for overlapped clusters at different rate [37] and FCM was seen better for most of the situations. Thus, it was decided to use FCM algorithm (See Appendix B) provided in Fuzzy Logic Toolbox of MATLAB to cluster our experimental groups by using selected features at previous step.

4. RESULTS

The algorithmic approach mentioned before was applied for each dataset (i.e. control, migraine, ADHD and Schizophrenia) and then pairwise clustering results are reported with following indexes. Frequency and location information of determined features, which are used to cluster chosen datasets, is also visualized as well as clustering results.

- **Precision:** $\text{True Positive} / (\text{True Positive} + \text{False Positive})$
- **Recall (Sensitivity):** $\text{True Positive} / (\text{True Positive} + \text{False Negative})$
- **True Negative Rate (Specificity):** $\text{True Negative} / (\text{True Negative} + \text{False Positive})$
- **Accuracy (Success):** $\text{True Positive} / (\text{True Positive} + \text{True Negative} + \text{False Positive} + \text{False Negative})$
- **Dunn's Index:** For well-separated clusters, distances among the clusters are usually large and the diameters of the clusters are small. Larger value means better cluster configuration [38].
- **Davies Bouldin Index:** Measurement of the average of similarity between each cluster and its most similar one. Compact and well-separated clusters lowers Davies-Bouldin index[38].

In addition to pairwise results, all datasets were used together to see how they can be discriminated from others. Then the success ratio and corresponding mixing matrix are reported.

Table 4.1
Illustration of True/False and Positive/Negative terms

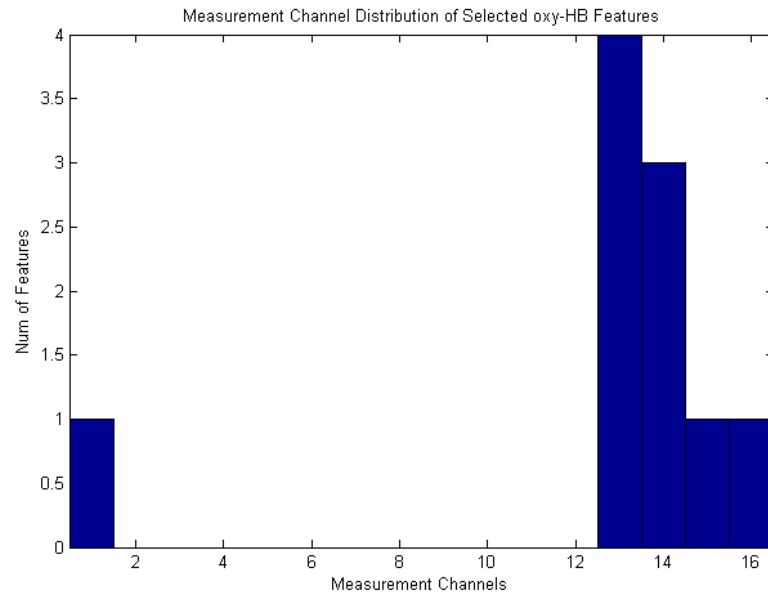
		Actual Class	
		TP Correct Result	FP Unexpected Result
Predicted Class	FN Missing Result	TN Correct Absence of Result	

4.1 Results for Control vs. Migraine Groups

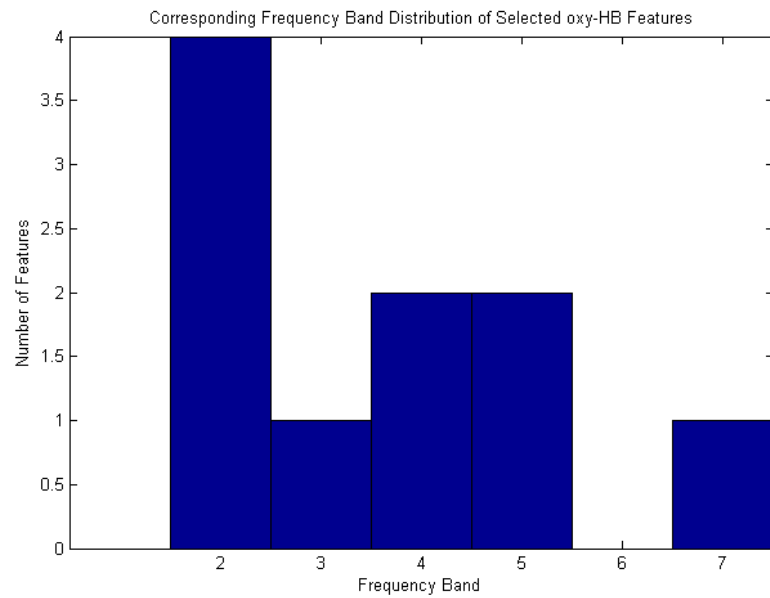
Clustering results for control and migraine groups are summarized in table 4.2. It can be observed that extracted and selected features from HbO_2 signal set is more suitable for discrimination of these groups since it gives better results than both Hb and HbT depended clustering. Additionally, these features are much related with right side of the prefrontal cortex (channels 13, 14, 15 and 16) and they are mostly corresponding to components which are dominant on 0.1-0.2 Hz and 0.3-0.5 Hz (bands 2, 4 and 5) (see figure 4.1).

Table 4.2
Clustering indexes for control & migraine groups

Signal Set	Accuracy	Sensitivity	Specificity	Precision	Dunn's Index	D-B Index
HbO₂	0.82	0.87	0.77	0.81	0.2144	0.0363
Hb	0.79	0.87	0.69	0.76	0.3526	0.0560
HbT	0.71	0.93	0.46	0.66	0.2987	0.4837

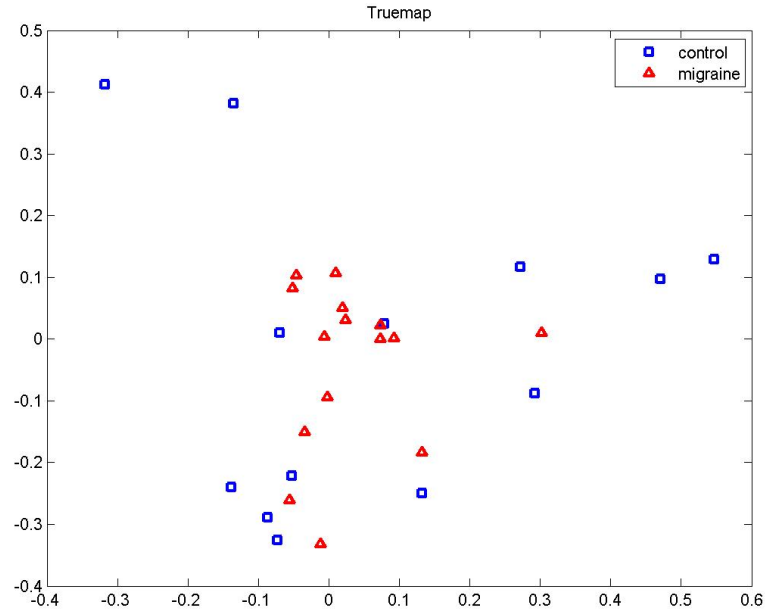


(a)

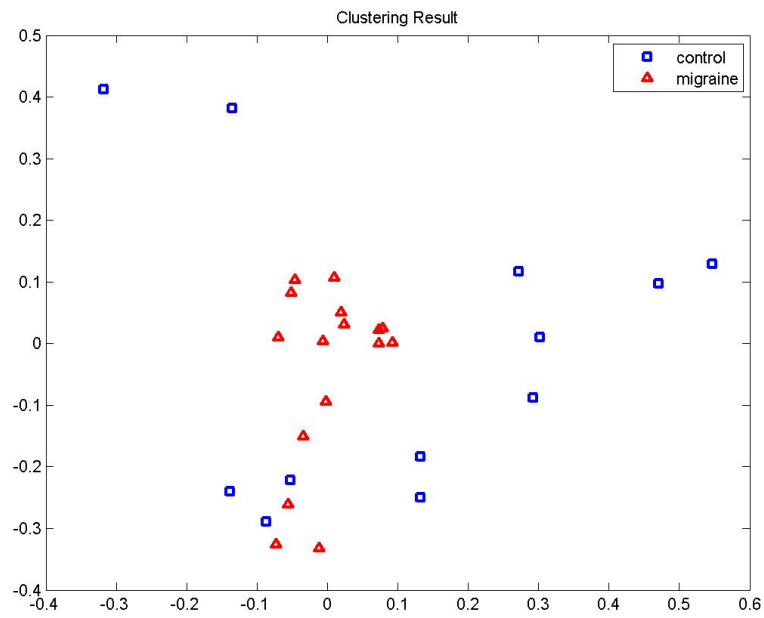


(b)

Figure 4.1 Channel distribution (a) and frequency band distribution (b) of selected HbO_2 features for Control-Migraine discrimination



(a)



(b)

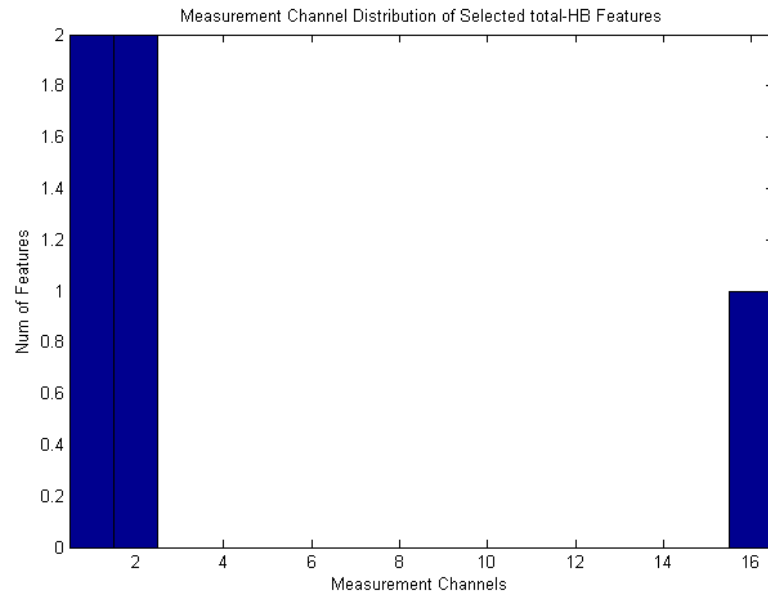
Figure 4.2 True map (a) and clustering result (b) based on selected HbO_2 features for Control-Migraine discrimination

4.2 Results for Control vs. Schizophrenia Groups

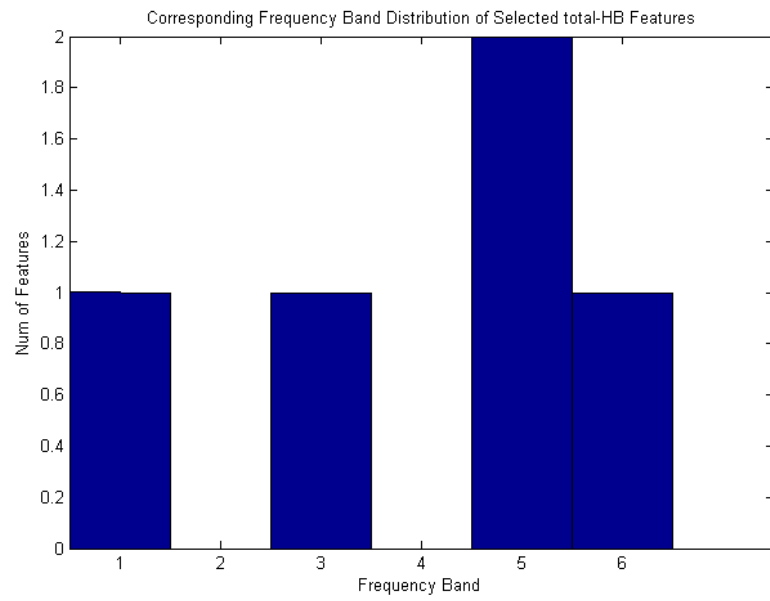
Clustering results for control and schizophrenia groups are summarized in table 4.3. It can be observed that features derived from all HbO_2 , Hb and HbT signal sets contain useful information for discrimination of these groups and they show almost equal performance in clustering step. Additionally, these features are much related with both right left side of the prefrontal cortex (channels 1, 2, 4, 14 and 16) and they are mostly corresponding to components which are much dominant on high frequencies (bands 3, 5 and 7) (see figure D.5, D.7 and 4.3).

Table 4.3
Clustering indexes for control & schizophrenia groups

Signal Set	Accuracy	Sensitivity	Specificity	Precision	Dunn's Index	D-B Index
HbO₂	0.87	0.85	0.92	0.96	0.2260	0.1178
Hb	0.85	0.85	0.85	0.91	0.0902	0.0196
HbT	0.92	0.96	0.85	0.93	0.0712	0.0446

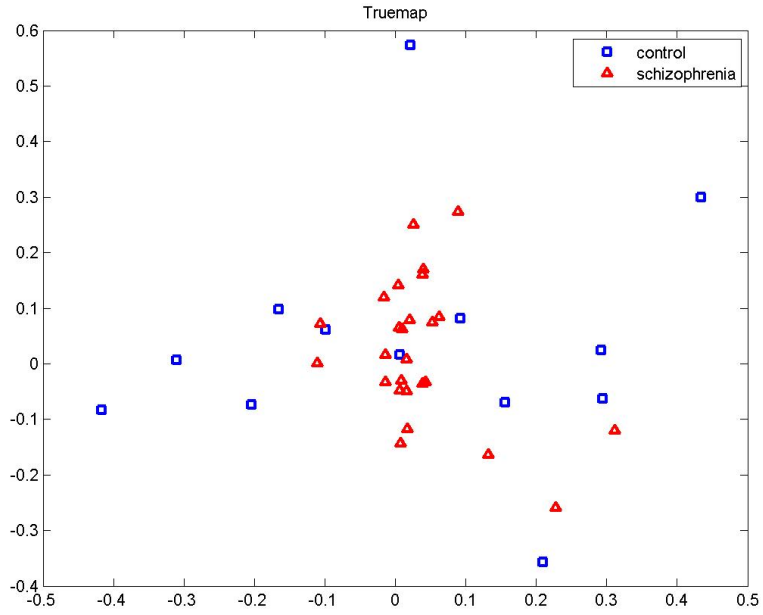


(a)

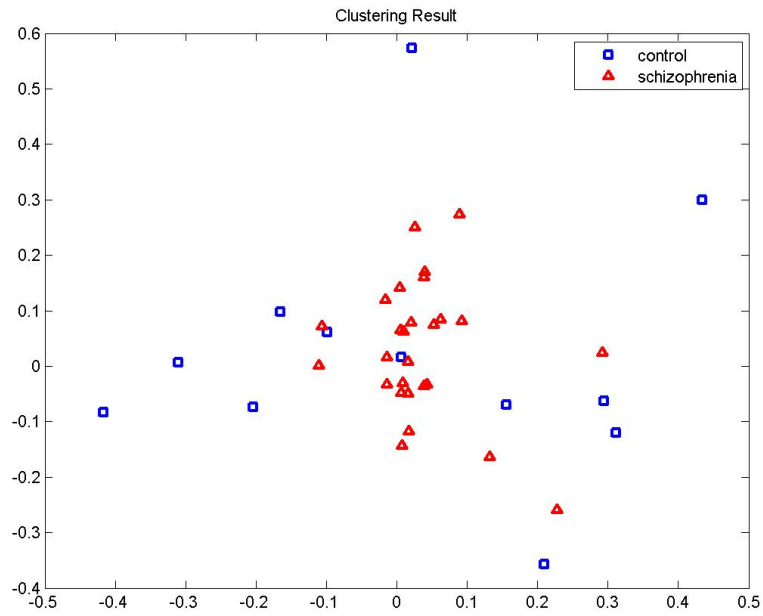


(b)

Figure 4.3 Channel distribution (a) and frequency band distribution (b) of selected *HbT* features for Control-Schizophrenia discrimination



(a)



(b)

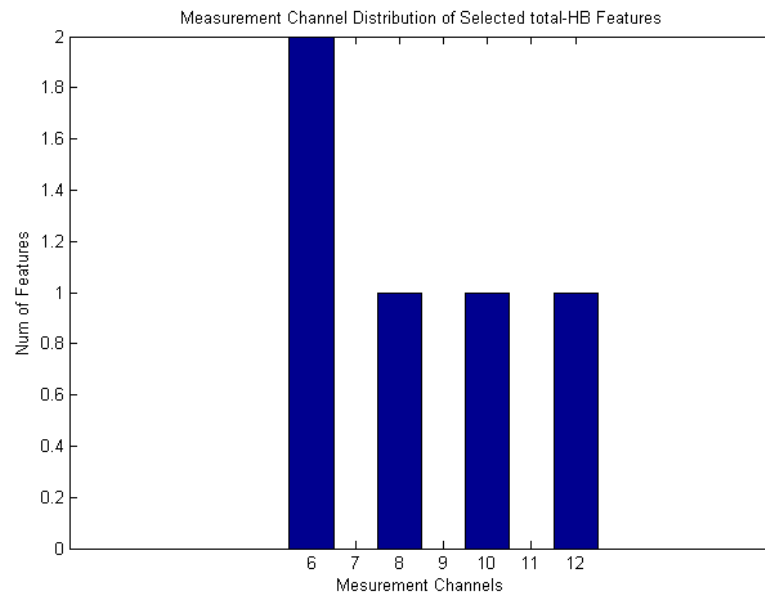
Figure 4.4 True map (a) and clustering result (b) based on selected *HbT* features for Control-Schizophrenia discrimination

4.3 Results for Control vs. ADHD Groups

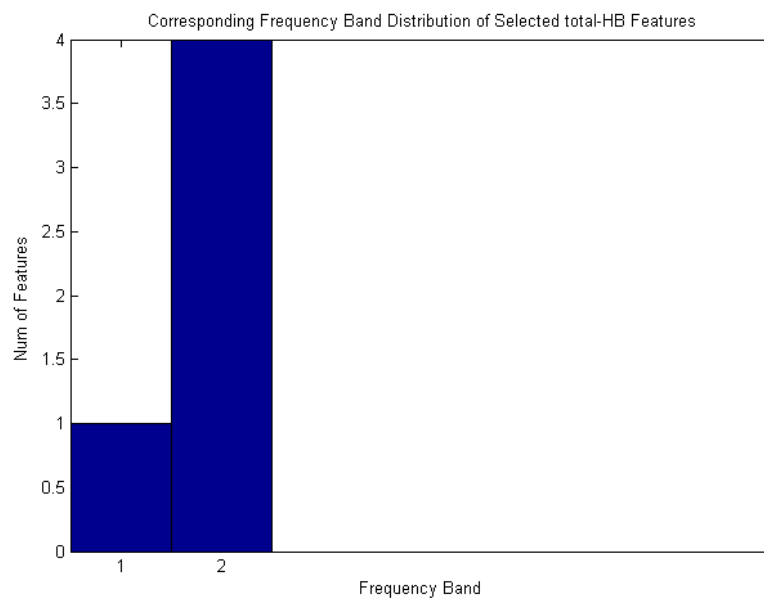
Clustering results for control and ADHD groups are summarized in table 4.4. It can be observed that extracted and selected features from *HbT* signal set is more suitable for discrimination of these groups since it gives better results than both *HbO₂* and *Hb* depended clustering. Additionally, these features are much related with middle region of the prefrontal cortex (channels 6, 8, 10 and 12) and they are mostly corresponding to components which are dominant on lower frequencies (bands 1 and 2) (see figure 4.5).

Table 4.4
Clustering indexes for control & ADHD groups

Signal Set	Accuracy	Sensitivity	Specificity	Precision	Dunn's Index	D-B Index
HbO₂	0.86	0.67	1	1	0.4489	0.0723
Hb	0.36	0.89	0	0.38	NA	NA
HbT	0.95	0.89	1	1	0.2187	0.0771

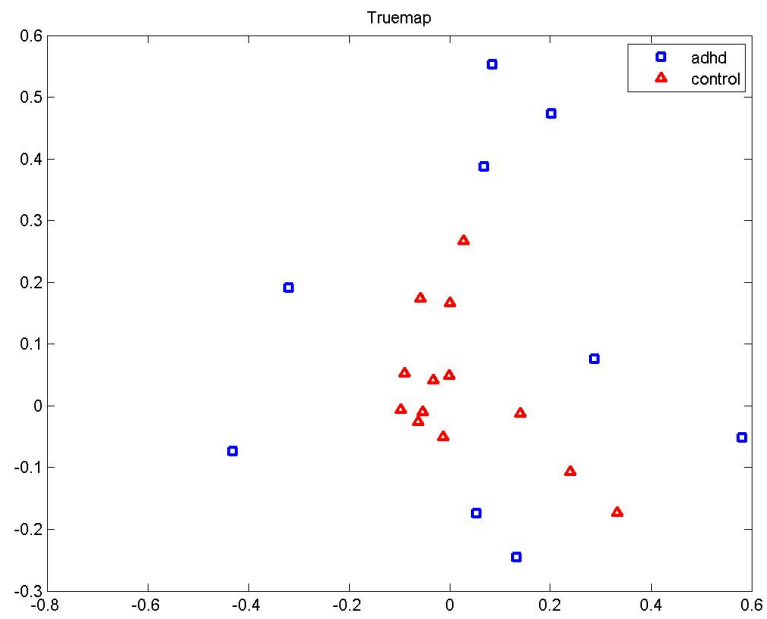


(a)

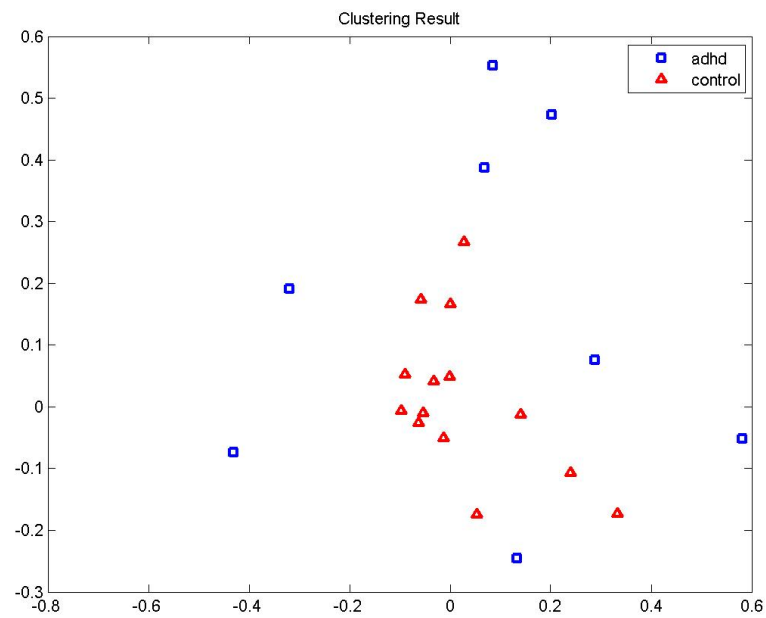


(b)

Figure 4.5 Channel distribution (a) and frequency band distribution (b) of selected *HbT* features for Control-ADHD discrimination



(a)



(b)

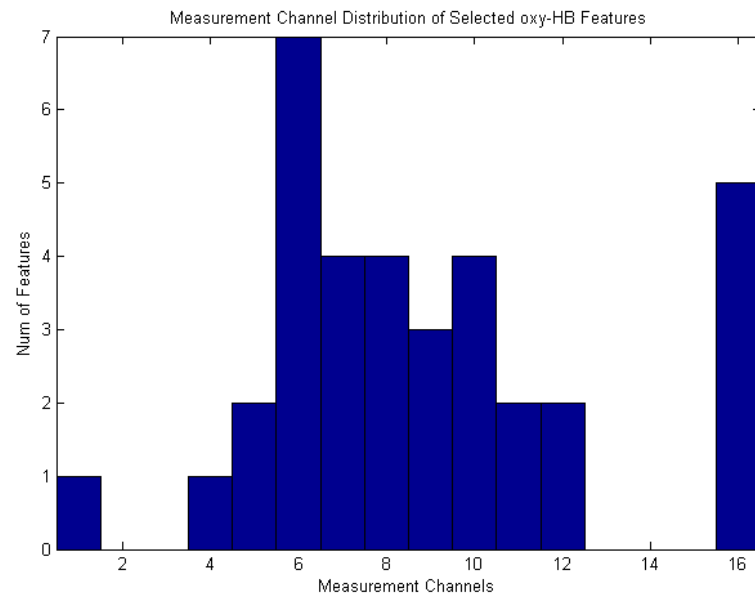
Figure 4.6 True map (a) and clustering result (b) based on selected *HbT* features for Control-ADHD discrimination

4.4 Results for Schizophrenia vs. Migraine Groups

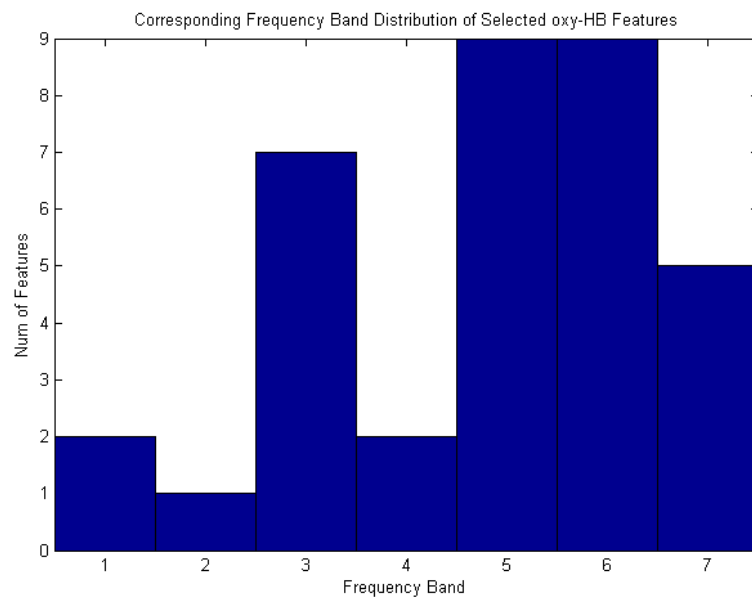
Clustering results for schizophrenia and migraine groups are summarized in table 4.5. It can be observed that extracted and selected features from HbO_2 signal set is more suitable for discrimination of these groups since it gives better results than both Hb and HbT depended clustering. Additionally, these features are much related with middle region of the prefrontal cortex (channels 6, 7, 8, 9 and 10) and they are mostly corresponding to components which are dominant on higher frequencies (bands 3, 5 and 6) (see figure 4.7).

Table 4.5
Clustering indexes for Schizophrenia & Migraine Groups

Signal Set	Accuracy	Sensitivity	Specificity	Precision	Dunn's Index	D-B Index
HbO₂	0.80	0.60	0.92	0.82	0.2402	0.0663
Hb	0.46	0.87	0.23	0.38	NA	NA
HbT	0.75	0.53	0.88	0.73	0.1481	0.3876

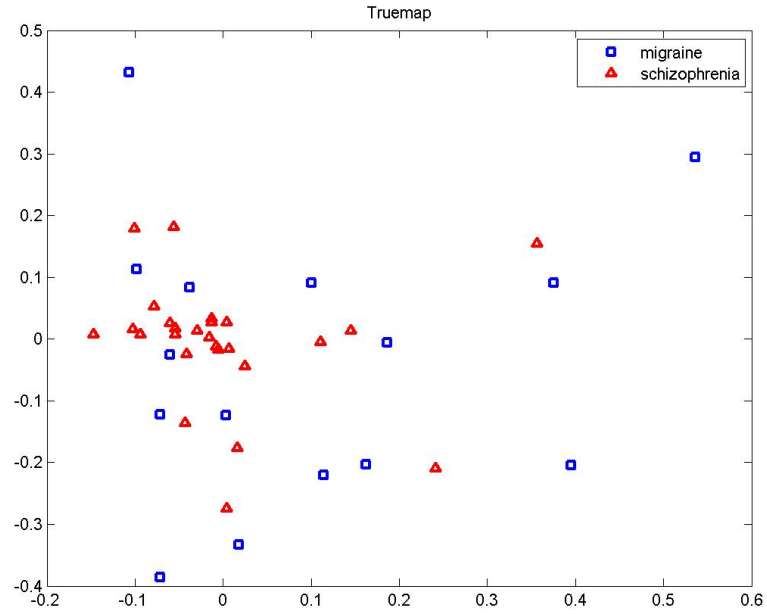


(a)

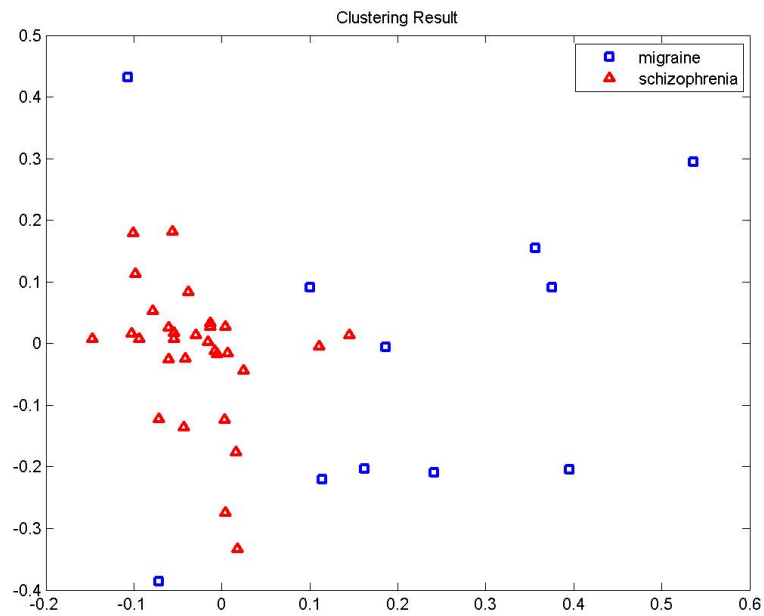


(b)

Figure 4.7 Channel distribution (a) and frequency band distribution (b) of selected HbO_2 features for Schizophrenia & Migraine discrimination



(a)



(b)

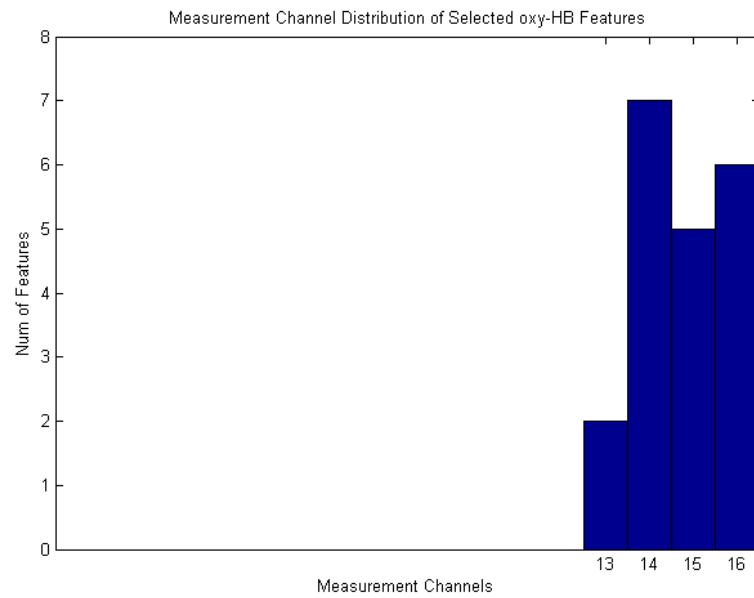
Figure 4.8 True map (a) and clustering result (b) based on selected HbO_2 features for Schizophrenia & Migraine discrimination

4.5 Results for ADHD vs. Migraine Groups

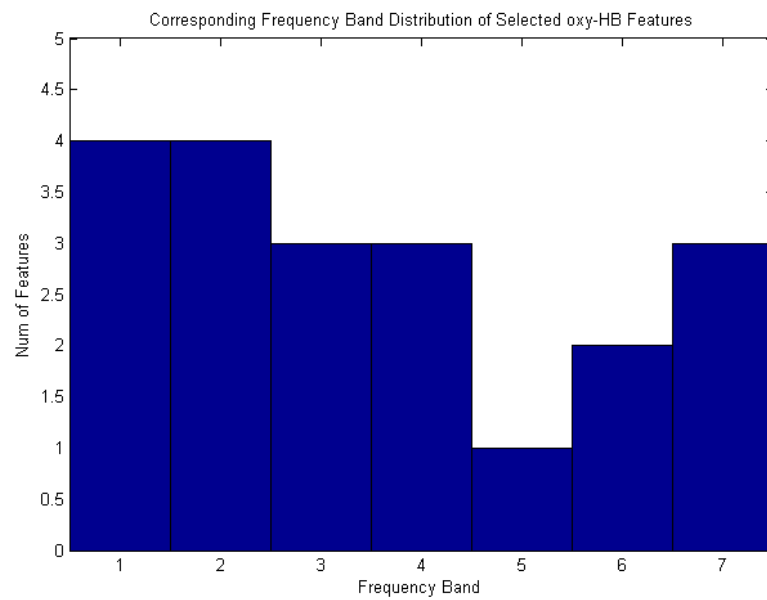
Clustering results for ADHD and migraine groups are summarized in table 4.6. It can be observed that extracted and selected features from HbO_2 signal set is more suitable for discrimination of these groups since it gives better results than both Hb and HbT depended clustering. Additionally, these features are much related with right side of the prefrontal cortex (channels 13, 14, 15 and 16) and frequency characteristics of these features does not focus on any specific interval (see figure 4.9).

Table 4.6
Clustering indexes for ADHD & migraine groups

Signal Set	Accuracy	Sensitivity	Specificity	Precision	Dunn's Index	D-B Index
HbO₂	0.88	0.87	0.89	0.93	0.1962	0.0877
Hb	0.83	0.94	0.67	0.82	0.3264	0.0062
HbT	0.88	0.93	0.77	0.88	0.2937	0.1195

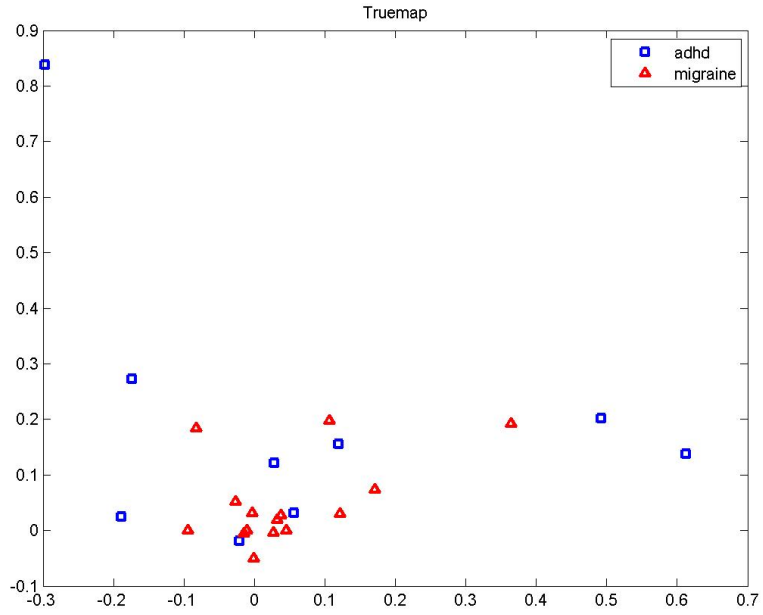


(a)

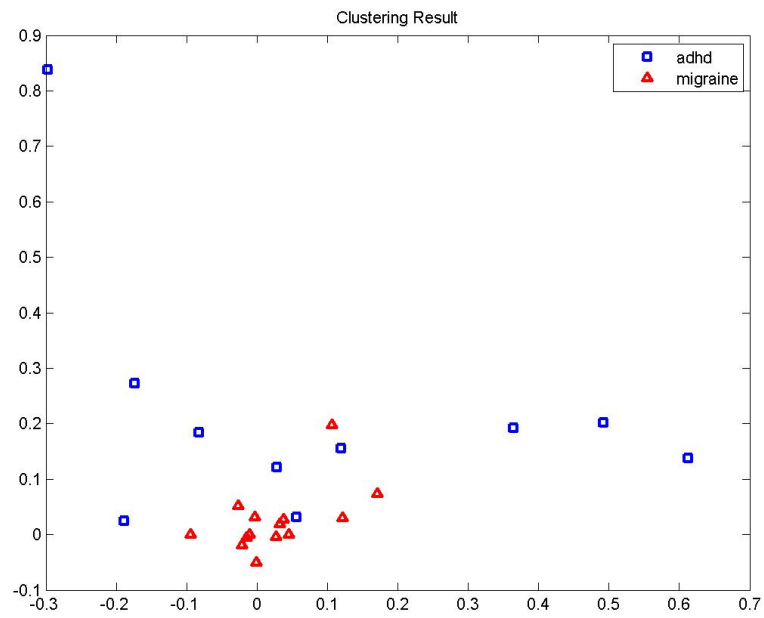


(b)

Figure 4.9 Channel distribution (a) and frequency band distribution (b) of selected HbO_2 features for ADHD-Migraine discrimination



(a)



(b)

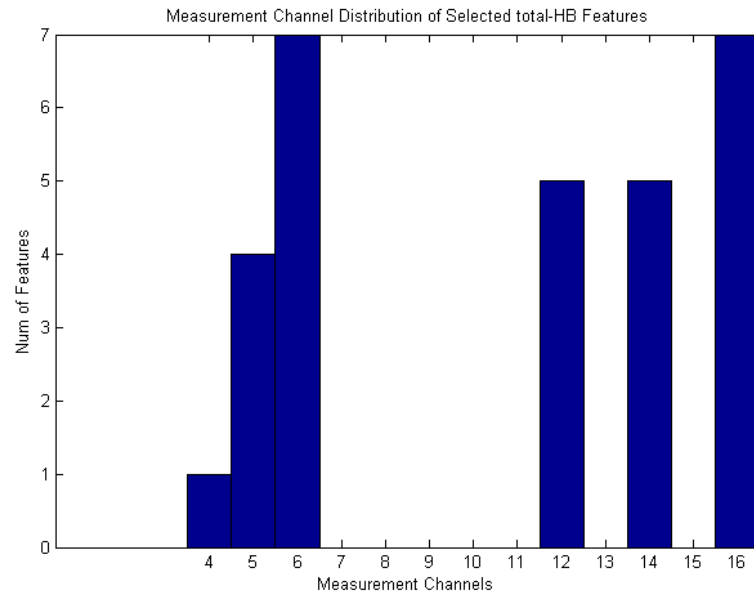
Figure 4.10 True map (a) and clustering result (b) based on selected HbO_2 features for ADHD-Migraine discrimination

4.6 Results for ADHD vs. Schizophrenia Groups

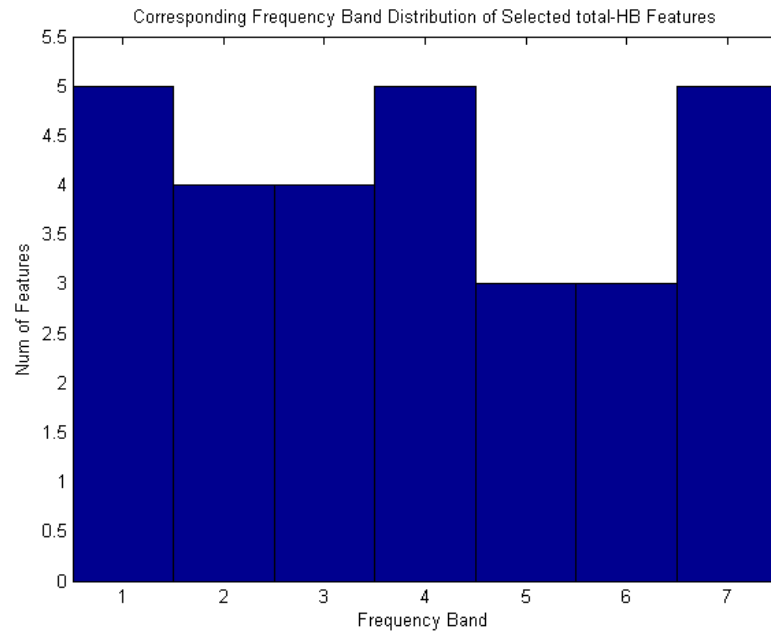
Clustering results for ADHD and migraine groups are summarized in table 4.7. It can be observed that extracted and selected features from HbO_2 and HbT signal sets are more suitable for discrimination of these groups since it gives better results than Hb depended clustering. Additionally, these features are much related with channels 5, 6, 14 and 16; and frequency characteristics of these features does not focus on any specific interval (see figures D.17 and 4.11).

Table 4.7
Clustering indexes for ADHD & schizophrenia groups

Signal Set	Accuracy	Sensitivity	Specificity	Precision	Dunn's Index	D-B Index
HbO₂	0.94	0.78	1	1	0.375	0.1194
Hb	0.83	0.67	0.89	0.67	0.3079	0.0347
HbT	0.94	1	0.92	0.82	0.1747	1.5602

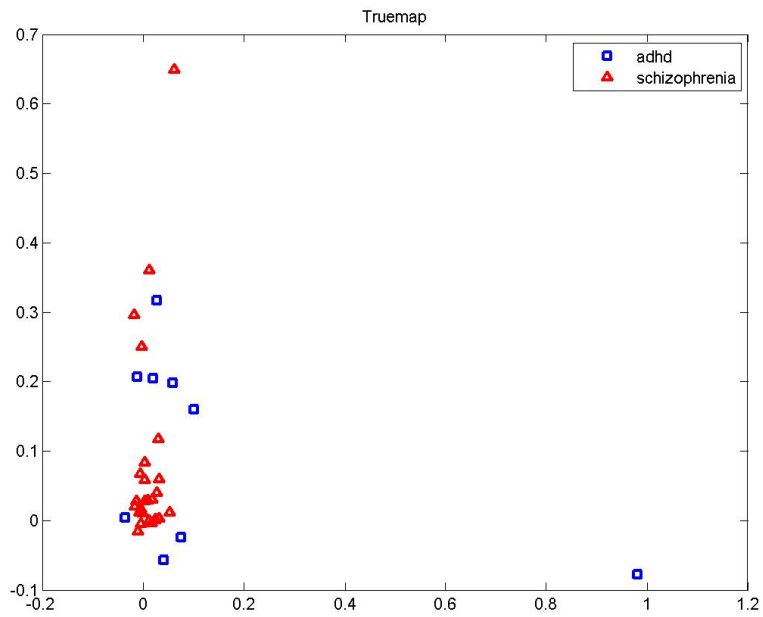


(a)

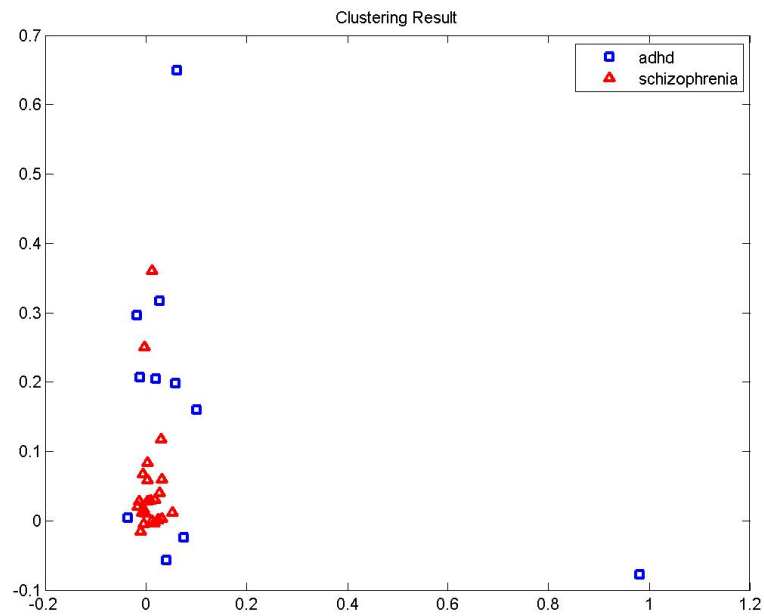


(b)

Figure 4.11 Channel distribution (a) and frequency band distribution (b) of selected *HbT* features for ADHD-Schizophrenia discrimination



(a)



(b)

Figure 4.12 True map (a) and clustering result (b) based on selected *HbT* features for ADHD-Schizophrenia discrimination

4.7 Results for Discrimination of All Groups Together

Mixing matrix of clustering results for discrimination of all groups are shown in tables 4.8, 4.9 and 4.10. It can be seen that success rate does not exceed 65% for any signal set. Additionally, extracted features are much related with 4th, 6th, 14th, 15th and 16th channels and frequency characteristics of these features does not focus on any specific interval (see figures D.21, 4.13 and D.23).

Table 4.8

Clustering results of selected HbO_2 features for all experimental groups together

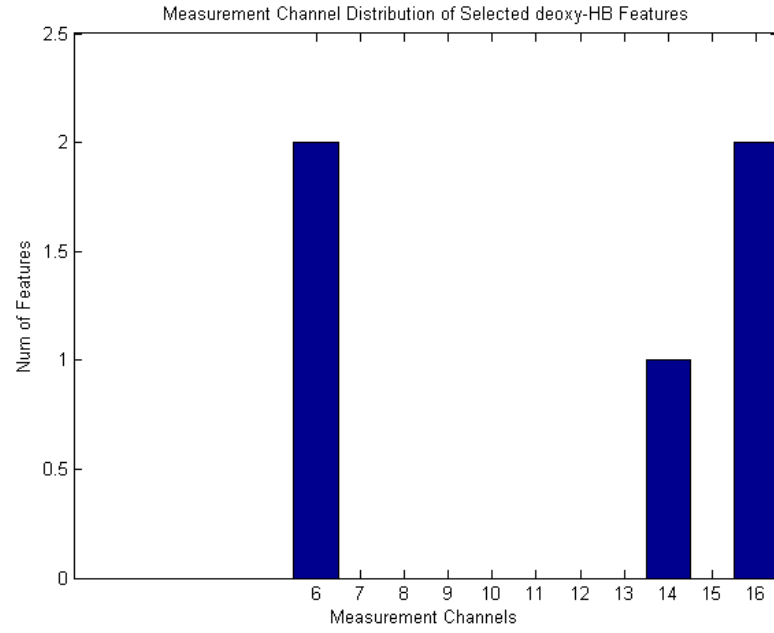
# of Subjects	HbO_2	Control	Migraine	Schizophrenia	ADHD
13	Control	12	-	1	-
15	Migraine	-	1	13	2
26	Schizophrenia	7	-	18	1
9	ADHD	1	-	1	7
	Accuracy: 0.60 Dunn's Index: 0.1896 D-B Index: 0.1467				

Table 4.9
Clustering results of selected *Hb* features for all experimental groups together

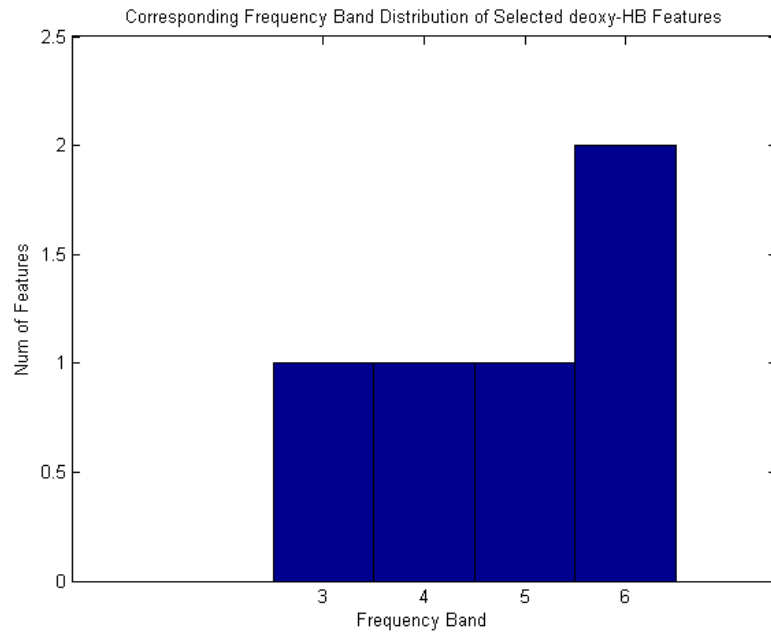
# of Subjects	<i>Hb</i>	Control	Migraine	Schizophrenia	ADHD
13	Control	8	3	1	1
15	Migraine	2	8	4	1
26	Schizophrenia	2	2	22	-
9	ADHD	3	2	1	3
	Accuracy: 0.65 Dunn's Index: 0.2052 D-B Index: 0.0397				

Table 4.10
Clustering results of selected *HbT* features for all experimental groups together

# of Subjects	<i>HbT</i>	Control	Migraine	Schizophrenia	ADHD
13	Control	11	-	2	-
15	Migraine	2	2	8	3
26	Schizophrenia	3	2	21	-
9	ADHD	4	1	-	4
	Accuracy: 0.60 Dunn's Index: 0.2701 D-B Index: 0.1803				

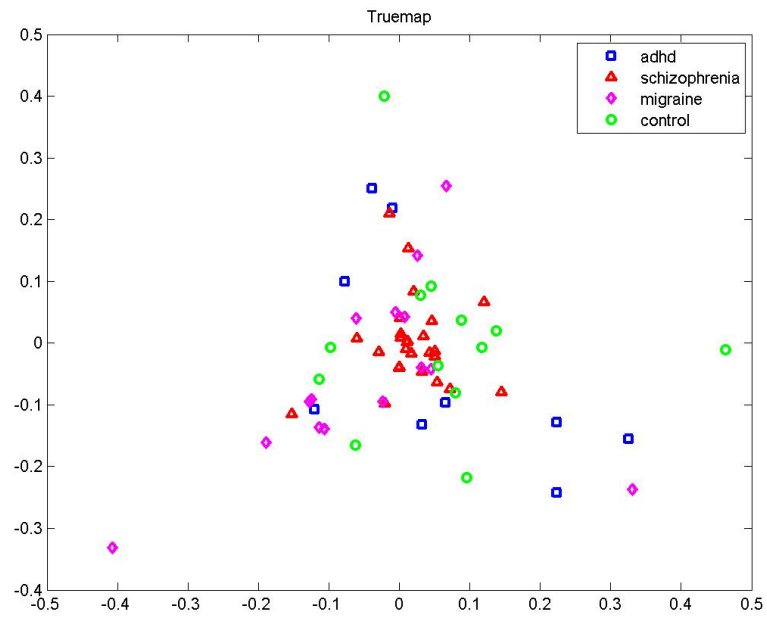


(a)

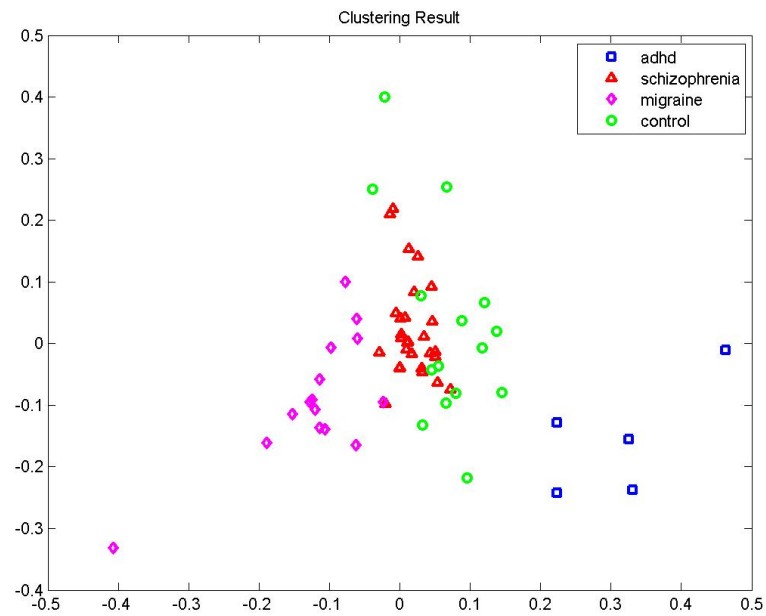


(b)

Figure 4.13 Channel distribution (a) and frequency band distribution (b) of selected *Hb* features for discrimination of all groups



(a)



(b)

Figure 4.14 True map (a) and clustering result (b) based on selected *Hb* features for discrimination of all groups

5. DISCUSSIONS

ICA has been commonly used to detect and remove artifacts from multivariate signal sets and researchers reported that it shows a better performance for removing artifacts from biosignals compared to other filtering or regression-based techniques [39, 34, 40]. The main reason of its high performance for finding these artifacts is its ability to recognize different patterns in multivariate signal sets. In some studies, ICA appears as a purposive tool to discriminate patterns which correspond to changes in a situation. For example, in a study by Formisano et al. [25] features extracted from task related IC's of fMRI dataset were used in automatic classification algorithm where they obtained high true-positive rate. In a study by Lu et al. [41], depressed people have been discriminated from healthy people with respect to their MEG signals. They compared Multi-channel Matching Pursuit algorithm to ICA to extract features and evaluated their performance. Furthermore, Storti et al. [42] use frequency information of independent components to investigate resting state networks in an fMRI study. They grouped IC's based on their dominancy of determined frequency intervals and use required IC's to extract these networks. In my case, IC's were ranked based on their spectral powers for determined frequency intervals and a feature set for each subject was extracted based on these spectral information coding the IC's to be used in the clustering step.

With inspiration from these studies, I decided to use ICA to extract features corresponding to common patterns which were specific for different PFC related diseases; namely schizophrenia, ADHD, and migraine.

In the study of Azechi et al. [5] schizophrenia patients were discriminated from healthy subjects by evaluating HbO_2 changes from fNIRS measurements during cognitive tasks. 88% of 60 subjects were correctly classified. HbO_2 depended control-schizophrenia clustering results of my study is very close to their study and it was also shown that using HbT information improves the success rate up to 92%. Additionally,

Callicot et al. reported abnormal activity of dorsal PFC under specific conditions in an fMRI study [11]. In my results, we observed that features effectively used to discriminate schizophrenia patients are much related with rightmost and leftmost parts of the fNIRS probe which are the closest locations of the probe to dorsal PFC (see figure 4.3).

In the study of Negoro et al. [4] ADHD patients exhibits less HbO_2 concentration change in fNIRS measurements during Stroop task and they reported HbO_2 changes in the control group is significantly greater than ADHD group in the inferior prefrontal cortex. Although there is not enough discrimination analysis during cognitive task in literature, activation differences between ADHD and control groups were reported during different tasks [4, 6, 22].

An fNIRS study that investigated migraine patients during a Stroop task reported no significant differences in amplitude of HbO_2 and Hb measurements [12]. However, Sayita completed a classification study in 2012 [30] and reported success rates up to 83% especially for HbT depended cases. Although experimental task which was used in my study is different from Sayita's, I reached to 82% accuracy for HbO_2 related analysis.

6. CONCLUSIONS

In this study, reflections of PFC related diseases on fNIRS measurements were investigated. It was seen that Schizophrenia, migraine and ADHD patients exhibit different alterations in fNIRS parameters which are hidden in these measurements. Signal processing technique used in this study helped us to differentiate disease specific fNIRS parameters. This new approach might increase the reliability of fNIRS usage for diagnostic purpose. Signal processing is an immense and ever-expanding research area. Therefore, choosing appropriate tools is essential to reach the goal of the study. For this reason, presented technique could be a start point for future studies to improve sensitivity and specificity of fNIRS for different cases.

In many of the previous fNIRS studies [8, 19, 5, 20, 6, 22, 23, 4, 30], the difference in the mean of the change in HbO_2 and Hb concentration were used to observe the discrimination power of fNIRS between one specific patient group and healthy controls. We challenged this approach by increasing the size and variety of the patient groups in this study. Furthermore, in contrast to most studies, we exploited the whole spectrum of the fNIRS signal for an improved accuracy. Although neuronal activity corresponds to low frequency part of fNIRS measurements, to understand meaning of high frequency content which seemed significantly effective on our results will be an important topic in future work.

Discrimination of control, migraine, schizophrenia and ADHD is evaluated both pairwise and all together, and then results were reported. It was seen that features derived from HbO_2 , Hb or HbT measurements could be useful to the show differences between these groups. Results also indicate that used patient groups can be differentiated from both control group and each other by choosing appropriate feature set.

Pairwise results for migraine show that they can be discriminated from other experimental groups with more than 80% of success and HbO_2 depended features come

into prominence. Results for schizophrenia indicate that these patients cannot be discriminated well from migraineurs, but evaluating them with control or ADHD patients gives more than 90% success rate. Clustering success for ADHD patients are relatively high than other results and *HbT* features gives better result during the study. However, ADHD Group is the smallest experimental group in this study and this may cause a bias on the results.

Clustering results shows more than 80% accuracy for at least one of the determined feature set for each pairwise analysis, but common features to cluster each experimental groups together does not exceed 65% success rate. It can be seen that selected common features cannot correctly discriminate migraine and schizophrenia patients. Although all our experimental groups consist of PFC related diseases, schizophrenia and ADHD are psychiatric diseases while migraine is a neurological disease. Therefore, evaluating them in the same pool could be inappropriate and may be the reason of this low success. Investigating discrimination of migraine and psychiatric diseases is another topic for future studies and it will be very assistive when explaining the meaning of our results.

fNIRS measurements may consist of different patterns for various experimental groups and this study proposed a novel analysis method to understand these differences. Although meaningful part of the fNIRS signals are constrained to low frequency information, we observed that high frequency components also carry valuable information for these patterns. Despite promising clustering results, extending database is necessity to reach much certain conclusion.

APPENDIX A. Independent Component Analysis

Steps of Fastica algorithm for one unit is shortly defined as following [36].

- Preprocessing for ICA

1. Centering x : Initial and the most necessary step is making x zero mean by subtracting its mean vector $m = E\{x\}$.

2. Whitening x : x is linearly transformed to obtain a new vector \tilde{x} which is white which means that covariance matrix of \tilde{x} is equal to identity matrix and components of \tilde{x} are uncorrelated.

$$E\{\tilde{x}\tilde{x}^T\} = I = EDE^T \quad (\text{A.1})$$

$$\tilde{x} = ED^{-1/2}E^T x \quad (\text{A.2})$$

- Main algorithm

1. Choose an initial weight vector w .
2. Let $w^+ = E\{xg(w^T x)\} - E\{g'(w^T x)\}w$ where $g(u) = \tanh(u)$.
3. Let $w = w^+ / \|w^+\|$
4. If not converged, go back to 2.

The one-unit algorithm estimates only one of the independent components. To estimate others, this algorithm is needed to run with weight vectors w_1, \dots, w_n . These vectors must be also decorrelated at each iteration to preventing from converging to the same maxima. This is achieved by subtracting the projections of the previously estimated n vectors from w_{n+1} and then normalizing w_{n+1}

$$w_{n+1} = w_{n+1} - \sum_{j=1}^n w_{n+1}^T w_j w_j \quad (\text{A.3})$$

$$w_{n+1} = w_{n+1} / \sqrt{w_{n+1}^T w_{n+1}} \quad (\text{A.4})$$

APPENDIX B. Feature Selection Algorithm

Here I will try to explain the algorithmic steps to define the features used in my thesis. The feature extraction can be applied to any type of fNIRS signal (i.e. $X = HbO_2$ or $X = Hb$, or $X = HbT$)

Algorithm 1 FSA Computation of the Feature Set

$k=1$; $\mathbf{F}[:, :] = \text{zeros}(7, 16)$

Calculate s_i from the ICA decomposition $X = AS$

Calculate power spectrum $P_i(f) = |\mathcal{FT}\{s_i(t)\}|^2$

Calculate the Power in frequency bands $P_i(B_k) = \sum_{f=f_L}^{f=f_H} P_i(f_L, f_H)$ where $B_k = (f_L, f_H)$ is given in Table.

Sort $P_i(B_k)$ and choose the highest one (i.e. j^{th} component).

$\mathbf{F}[k, :] = A[j, :]$

repeat

$k = k + 1$

until $k = 7$

return \mathbf{F}

APPENDIX C. Fuzzy C-Means Clustering

Fuzzy C-means algorithm is based on to minimize following objection function.[43]

$$J_m(U, v) = \sum_{k=1}^n \sum_{i=1}^c (u_{ik})^m d_{ik}^2, \quad (\text{C.1})$$

where $d_{ik}^2 = \| y_k - v_i \|^2$

Variables of Equation B1 are identified as below.

$Y = \{y_1, y_2, \dots, y_N\} \subset R^n = \text{data}$

$c = \text{number of clusters in } Y; 2 \leq c \leq n$

$m = \text{weighting exponent}; 1 \leq m \leq \infty$

$U = \text{fuzzy c-partition of } Y$

$$u_i(y_k) = u_{ik} = \begin{cases} 1 & y_k \in Y_i; \\ 0 & \text{otherwise} \end{cases}$$

$v = (v_1, v_2, \dots, v_c) = \text{vectors of centers}$

$v_i = (v_{i1}, v_{i2}, \dots, v_{ic}) = \text{centers of cluster } i$

- Main algorithm:

1. Fix c and m . Choose an initial matrix $U^{(0)}$
2. Compute $\hat{v}^{(k)}$ at step k according to

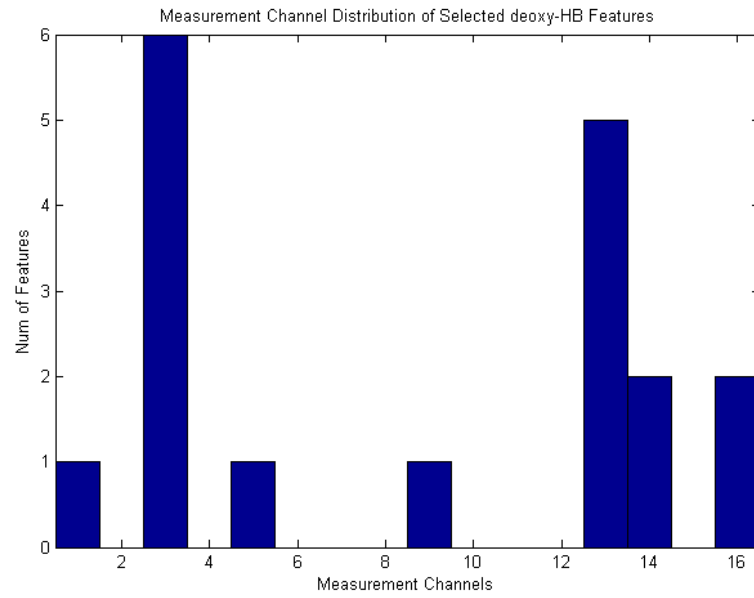
$$* \hat{v}_i = \frac{\sum_{k=1}^N (\hat{u}_{ik})^m y_k}{\sum_{k=1}^N (\hat{u}_{ik})^m}; 1 \leq i \leq c$$

3. Update membership matrix $\hat{U}^{(k+1)} = [\hat{u}_{ik}^{(k+1)}]$ according to

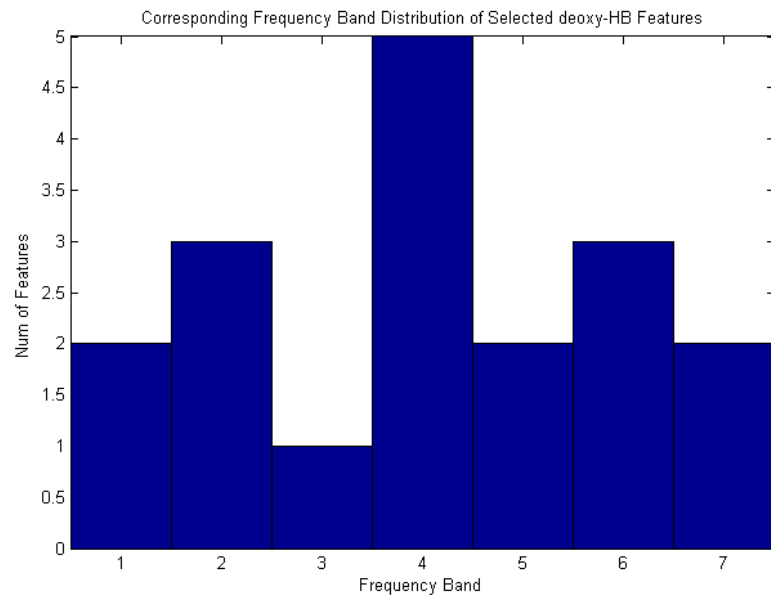
$$* \hat{u}_{ik} = \left(\sum_{j=1}^c \left(\frac{\hat{d}_{ik}}{\hat{d}_{jk}} \right)^{2/(m-1)} \right)^{-1}; 1 \leq k \leq N; 1 \leq i \leq c$$

4. If $\| \hat{U}^{(k+1)} - \hat{U}^{(k)} \| < \epsilon$, stop. Otherwise, set $\hat{U}^{(k)} = \hat{U}^{(k+1)}$ and return to (2)

APPENDIX D. Additional Figures for Results

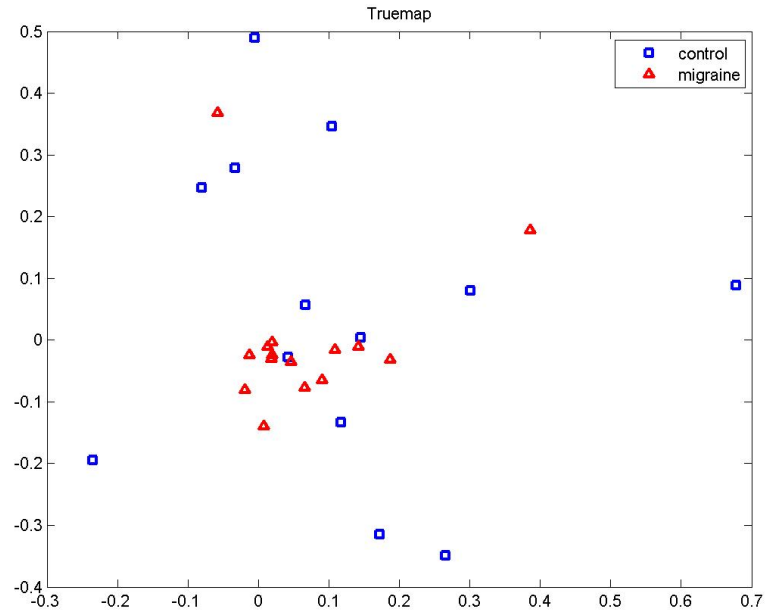


(a)

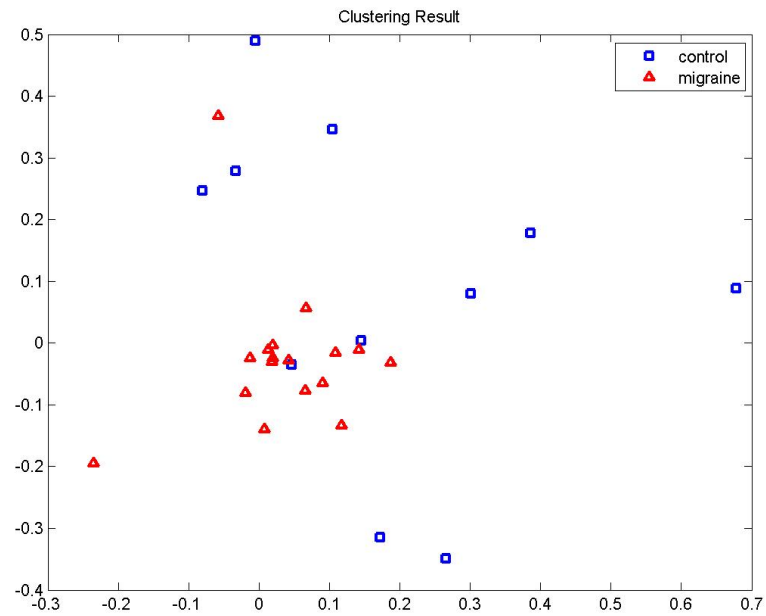


(b)

Figure D.1 Channel distribution (a) and frequency band distribution (b) of selected *Hb* features for Control-Migraine discrimination

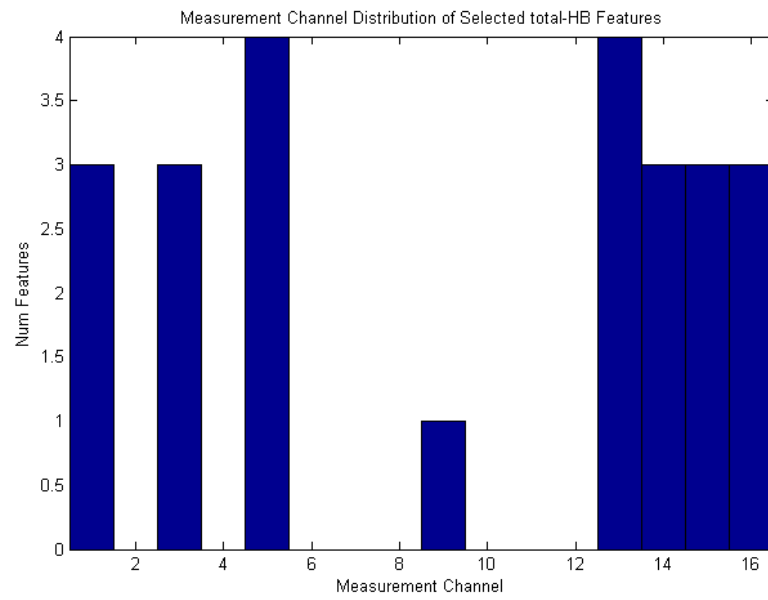


(a)

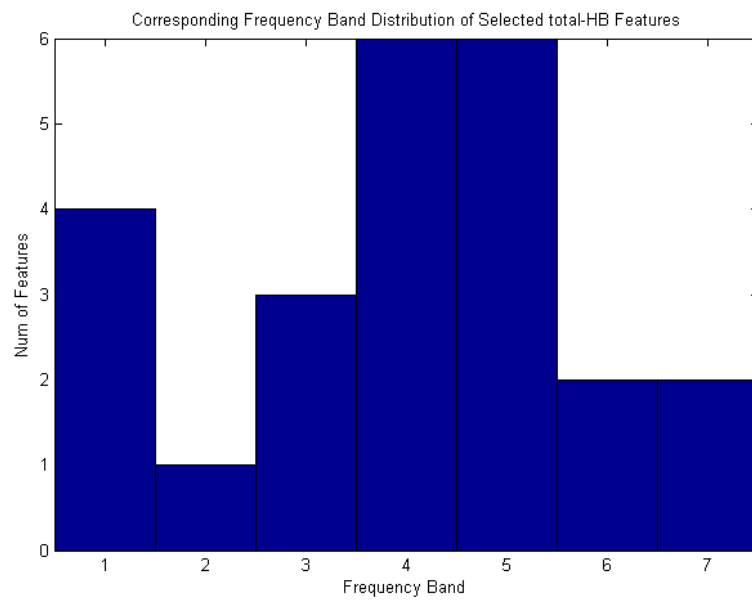


(b)

Figure D.2 True map (a) and clustering result (b) based on selected *Hb* features for Control-Migraine discrimination

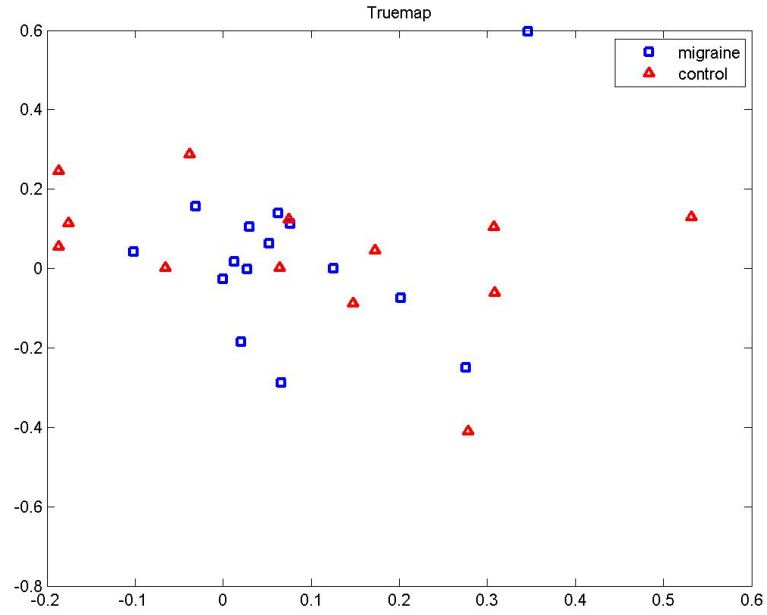


(a)

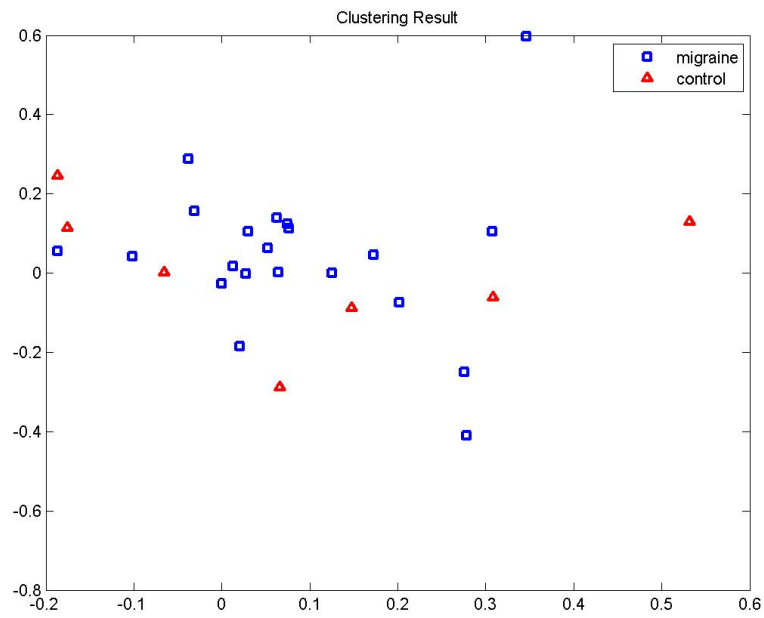


(b)

Figure D.3 Channel distribution (a) and frequency band distribution (b) of selected *HbT* features for Control-Migraine discrimination

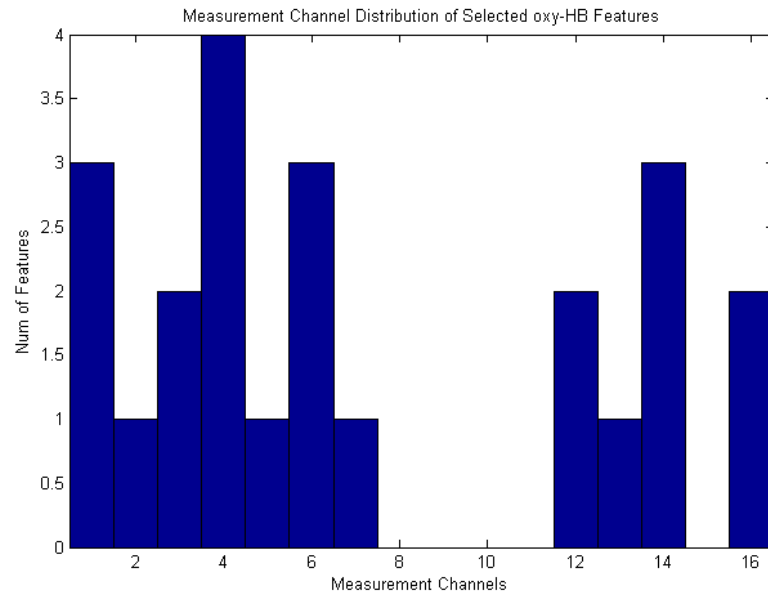


(a)

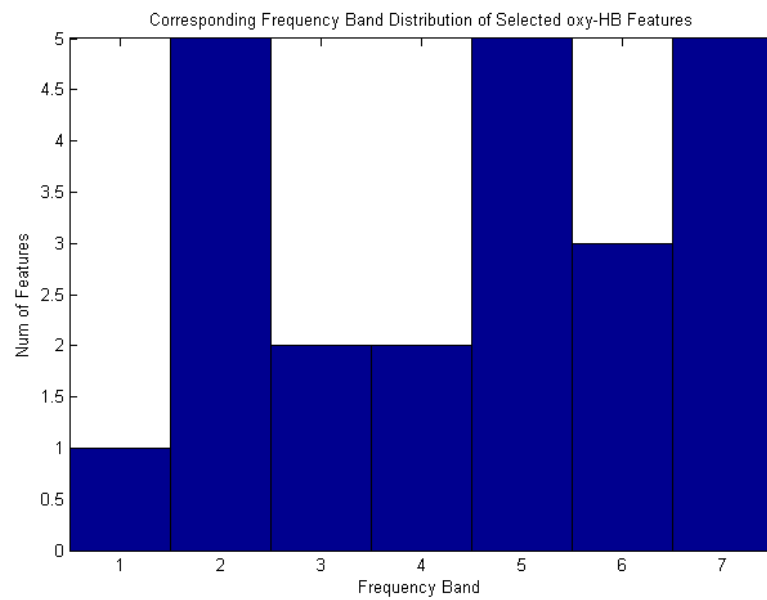


(b)

Figure D.4 True map (a) and clustering result (b) based on selected *HbT* features for Control-Migraine discrimination

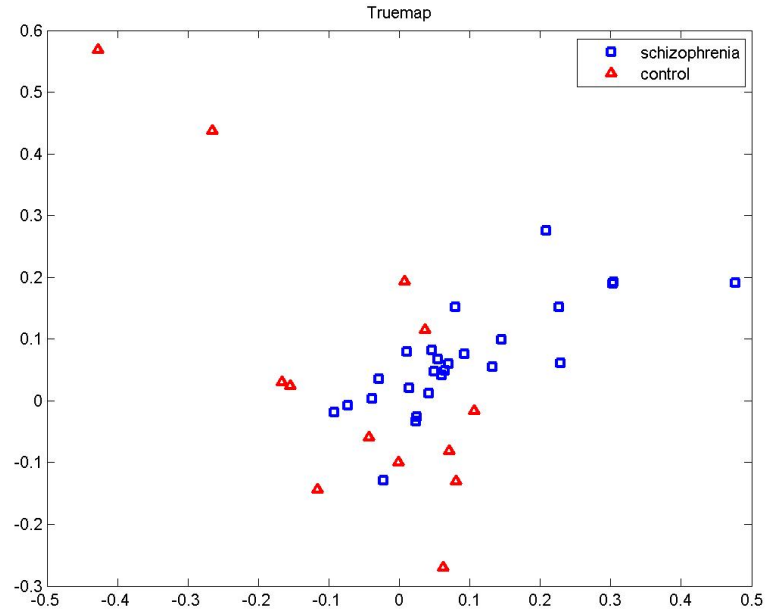


(a)

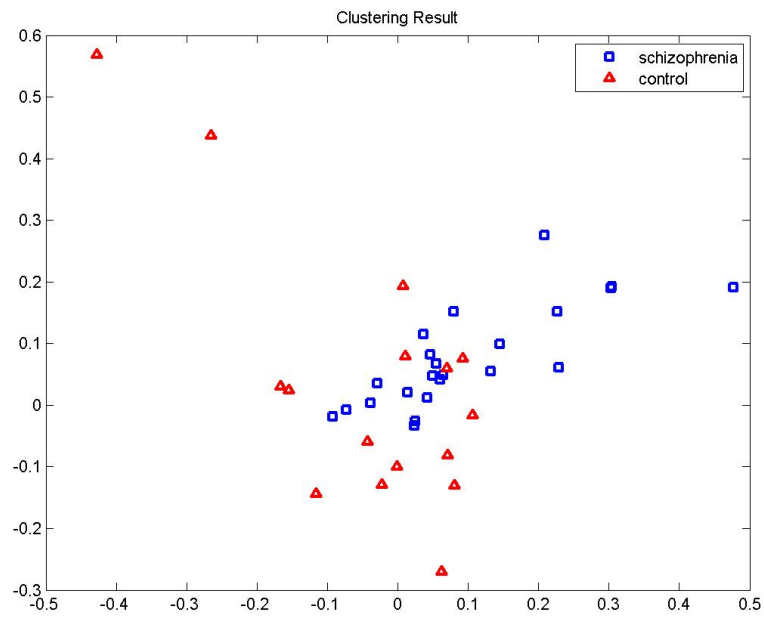


(b)

Figure D.5 Channel distribution (a) and frequency band distribution (b) of selected HbO_2 features for Control-Schizophrenia discrimination

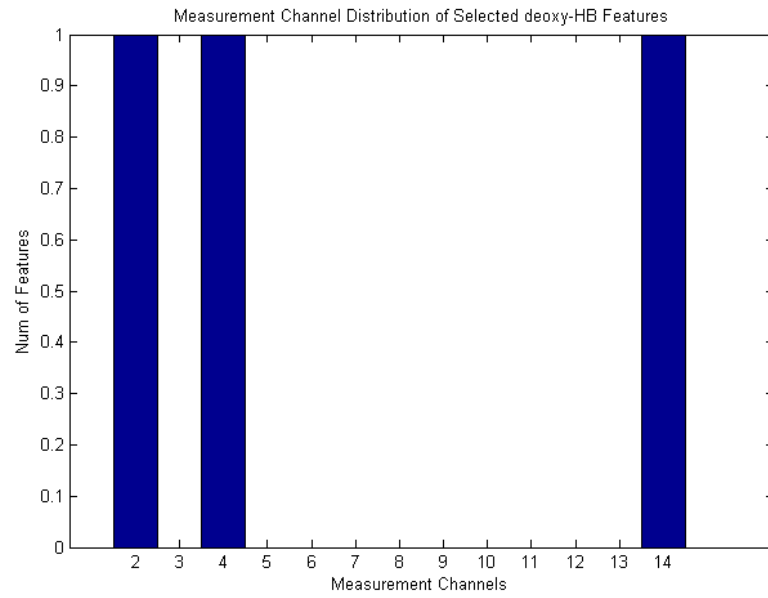


(a)

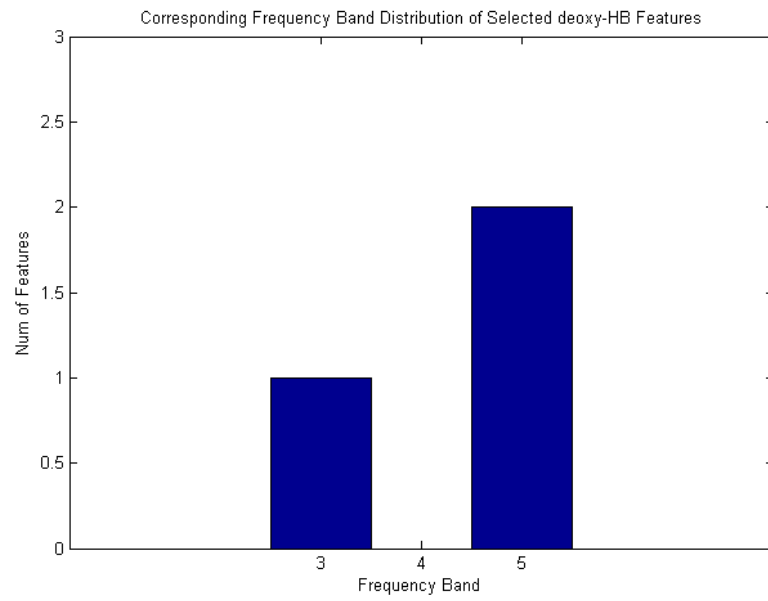


(b)

Figure D.6 True map (a) and clustering result (b) based on selected HbO_2 features for Control-Schizophrenia discrimination

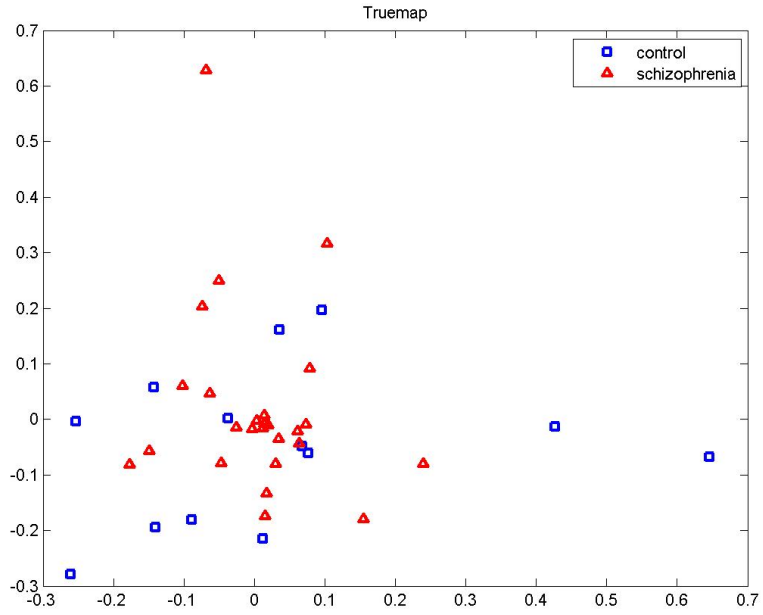


(a)

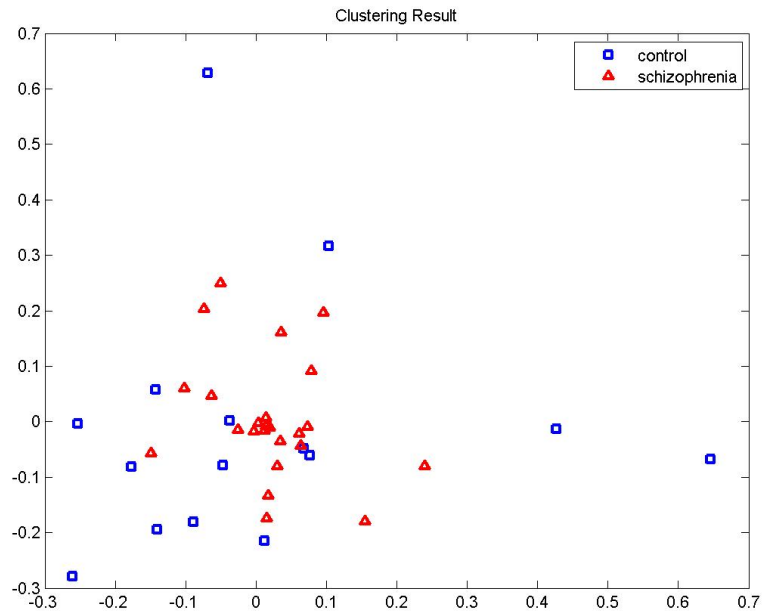


(b)

Figure D.7 Channel distribution (a) and frequency band distribution (b) of selected *Hb* features for Control-Schizophrenia discrimination

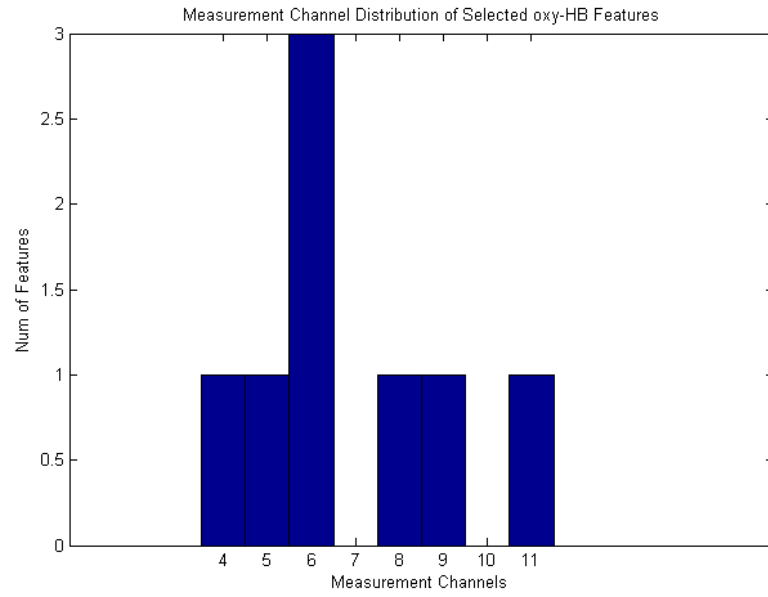


(a)

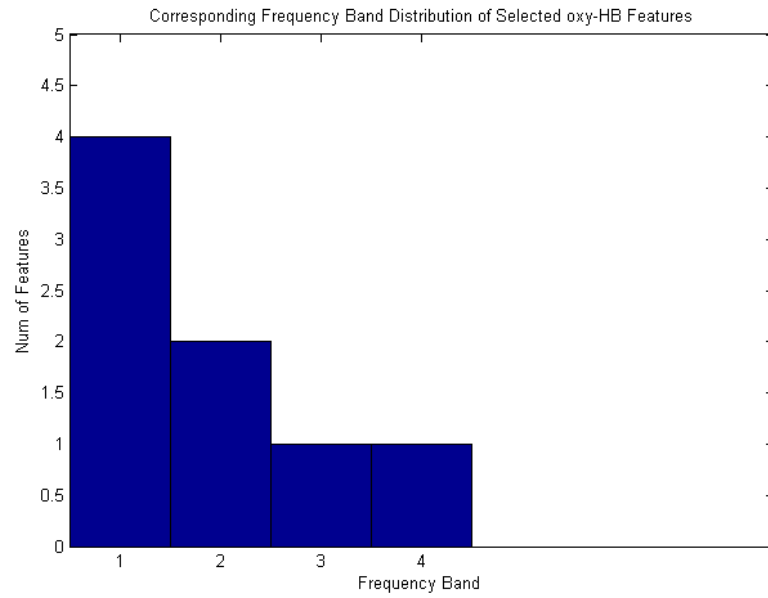


(b)

Figure D.8 True map (a) and clustering result (b) based on selected *Hb* features for Control-Schizophrenia discrimination

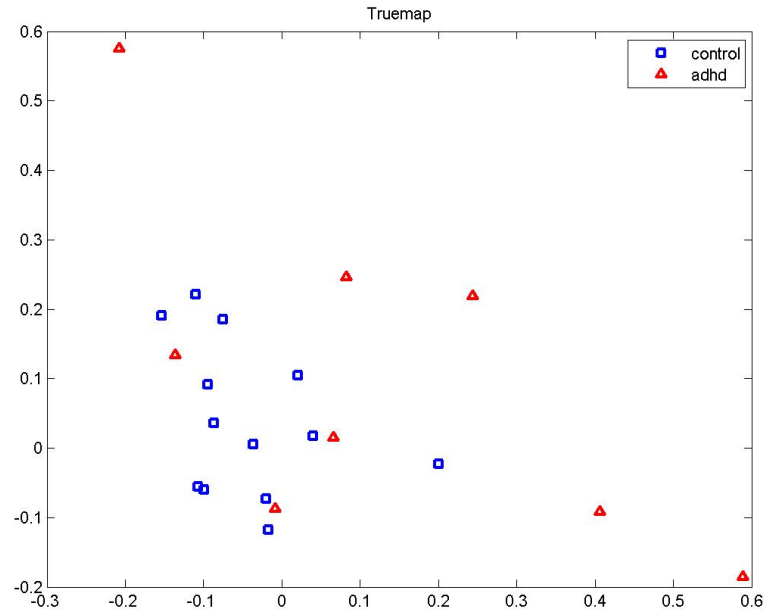


(a)

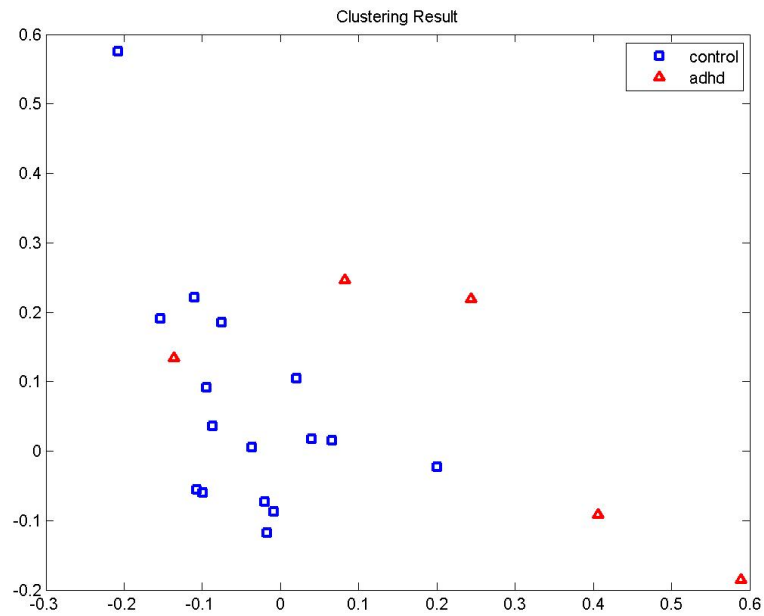


(b)

Figure D.9 Channel distribution (a) and frequency band distribution (b) of selected HbO_2 features for Control-ADHD discrimination

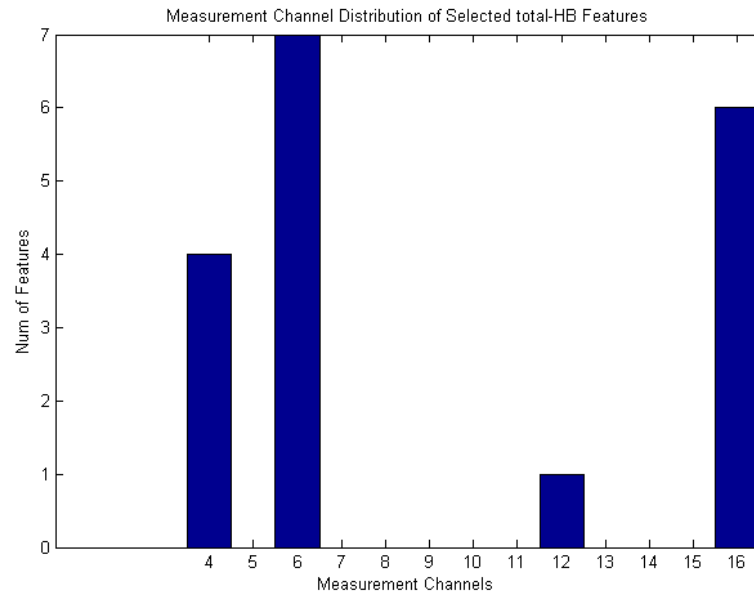


(a)

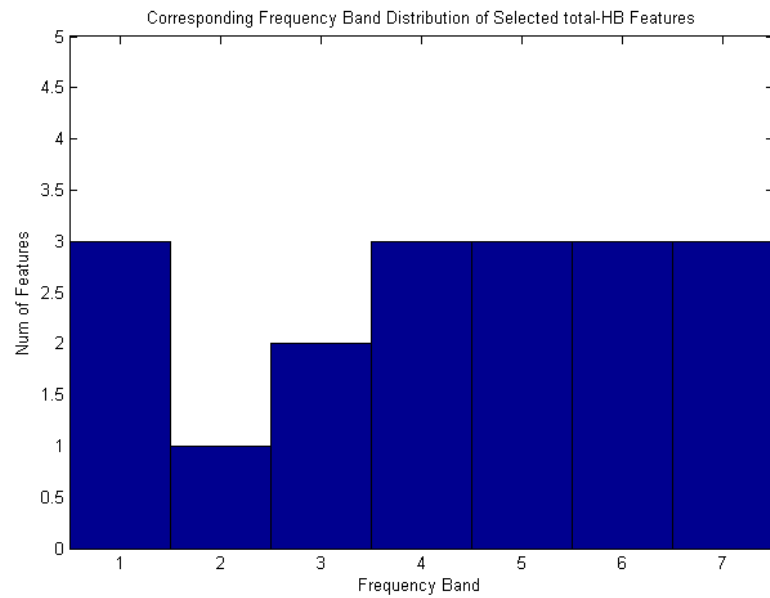


(b)

Figure D.10 True map (a) and clustering result (b) based on selected HbO_2 features for Control-ADHD discrimination

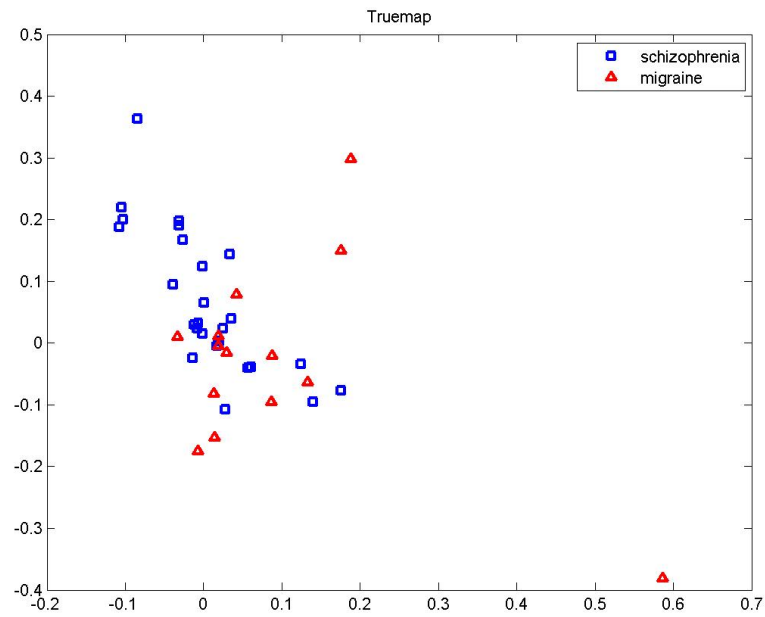


(a)

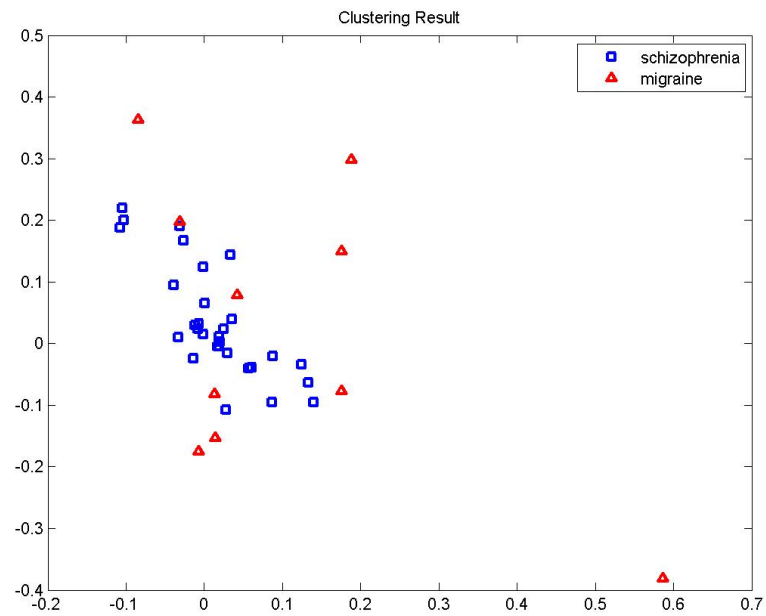


(b)

Figure D.11 Channel distribution (a) and frequency band distribution (b) of selected *HbT* features for Schizophrenia & Migraine discrimination

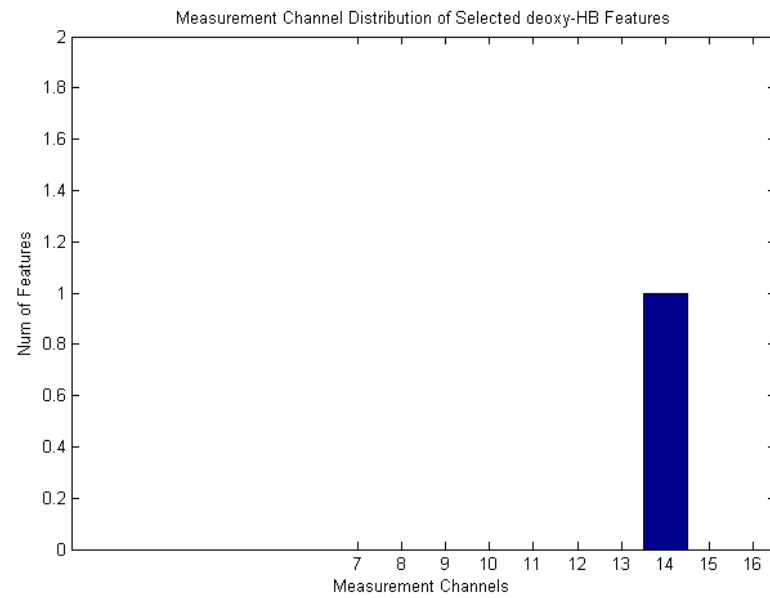


(a)

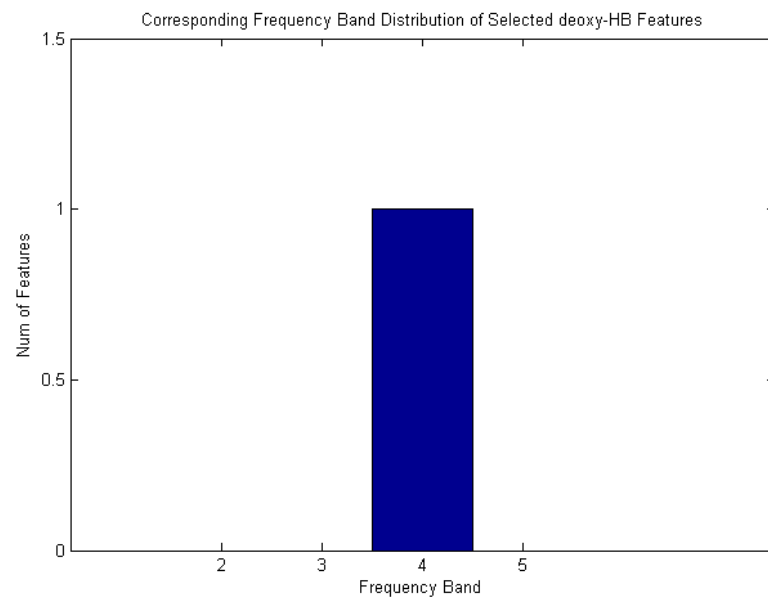


(b)

Figure D.12 True map (a) and clustering result (b) based on selected *HbT* features for Schizophrenia & Migraine discrimination

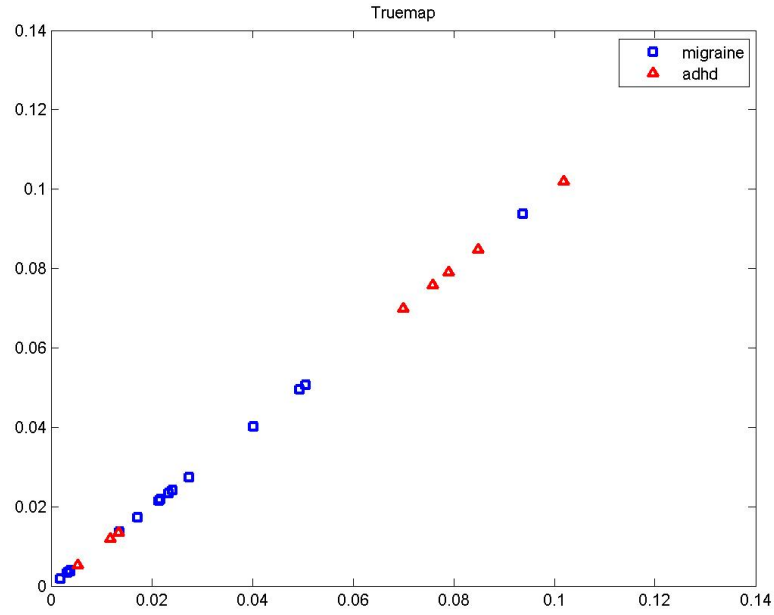


(a)

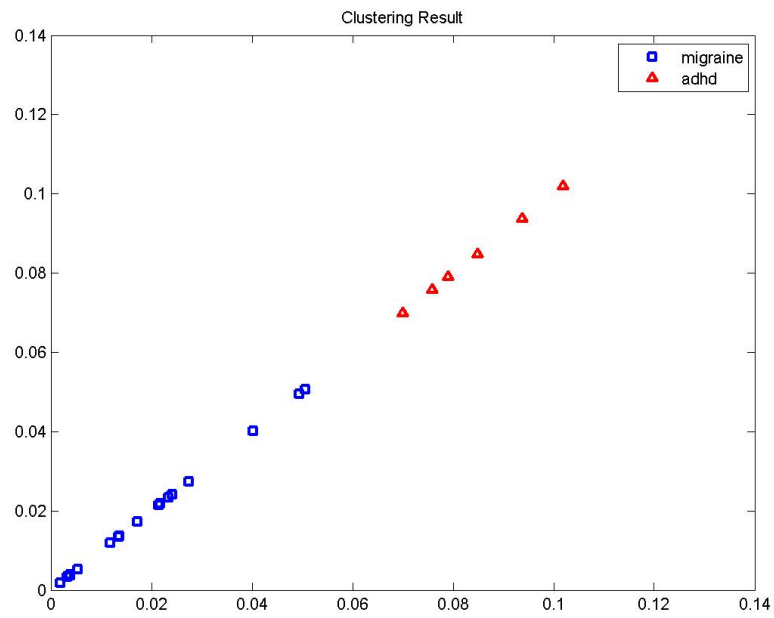


(b)

Figure D.13 Channel distribution (a) and frequency band distribution (b) of selected *Hb* features for ADHD-Migraine discrimination

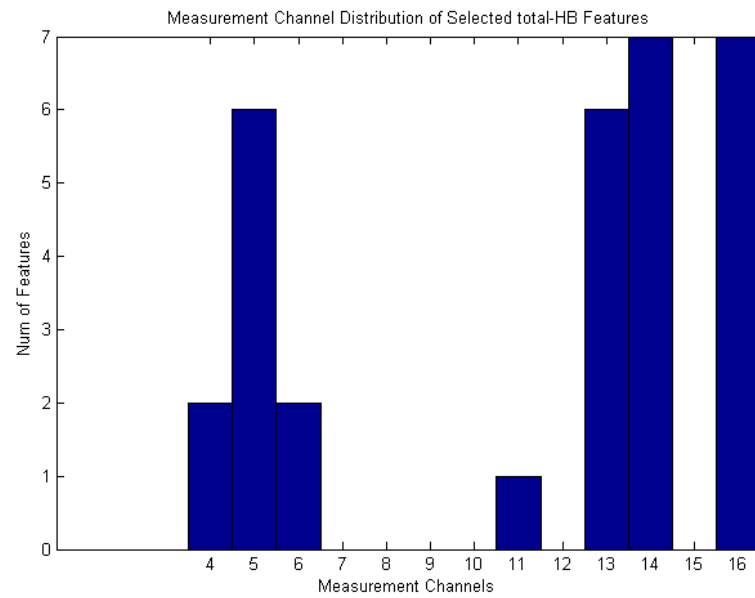


(a)

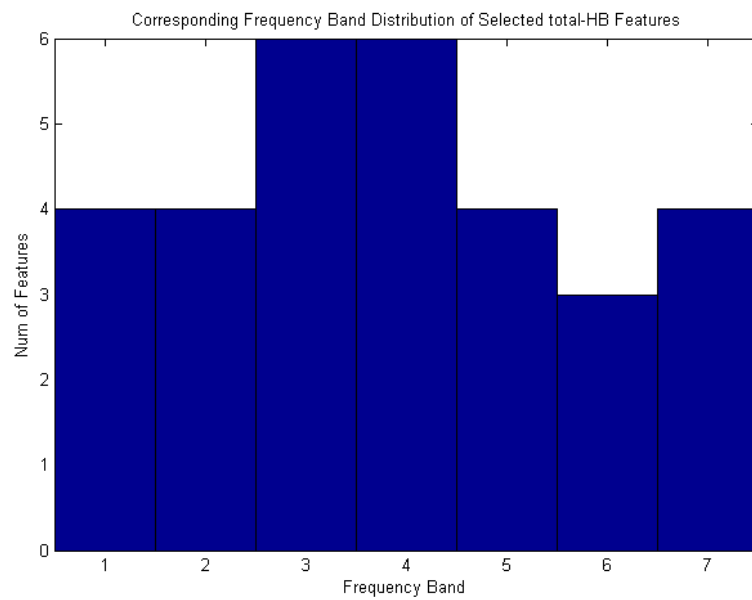


(b)

Figure D.14 True map (a) and clustering result (b) based on selected *Hb* features for ADHD-Migraine discrimination

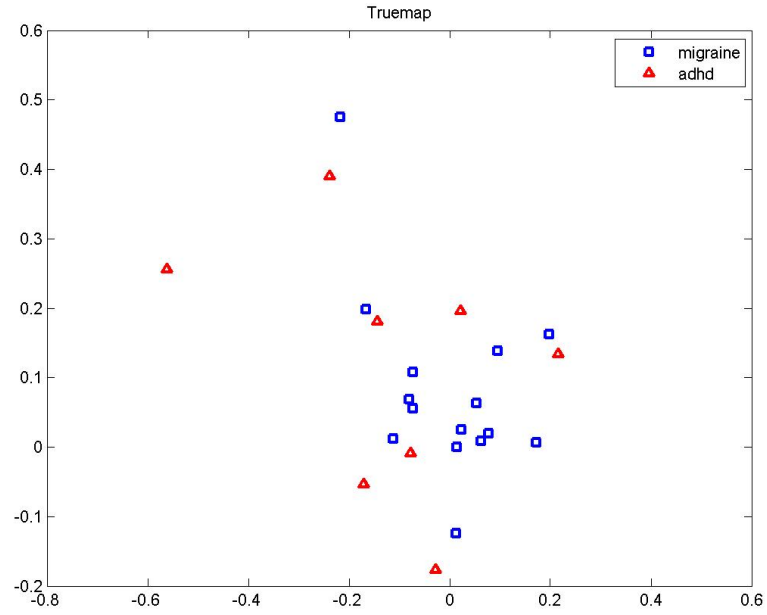


(a)

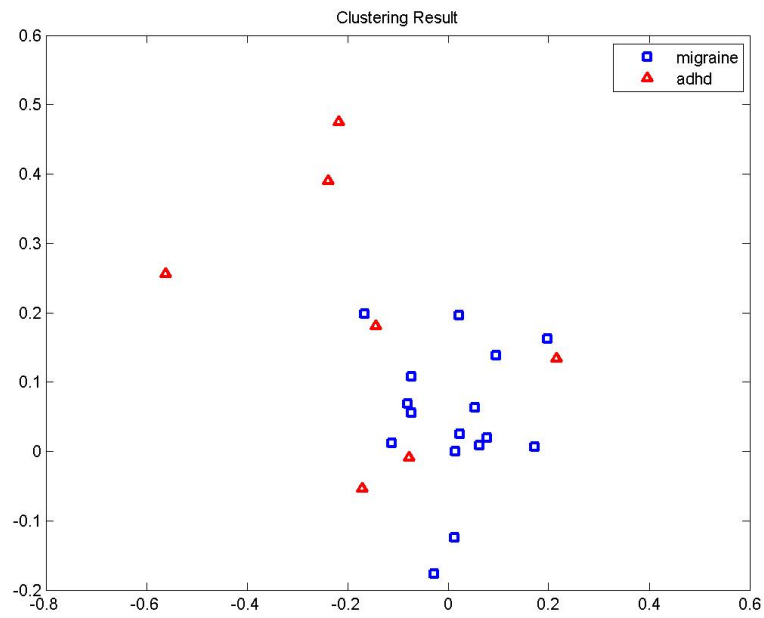


(b)

Figure D.15 Channel distribution (a) and frequency band distribution (b) of selected *HbT* features for ADHD-Migraine discrimination

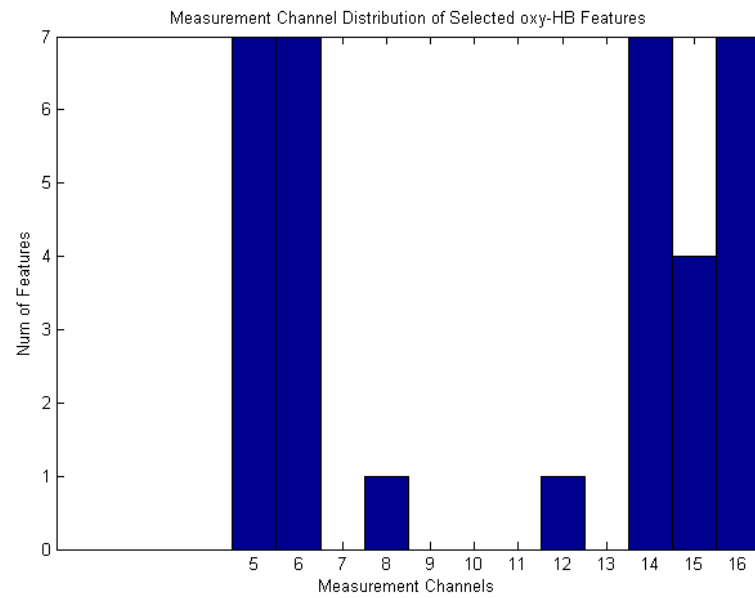


(a)

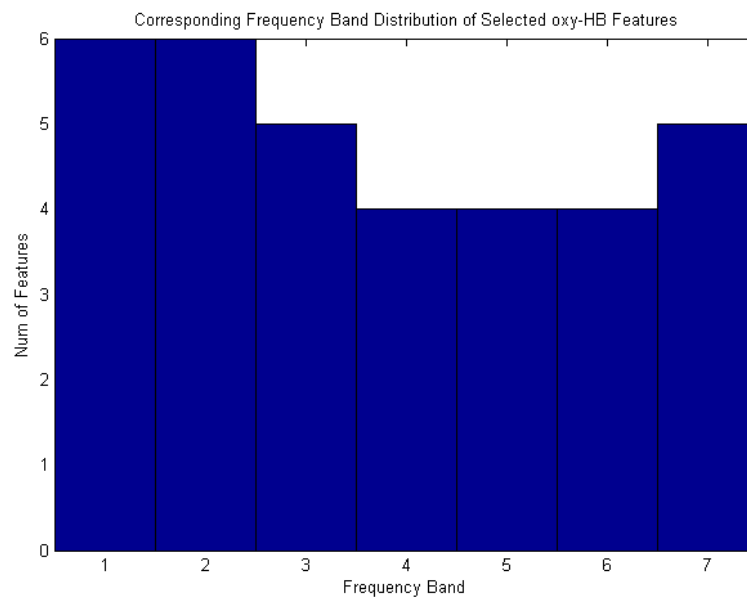


(b)

Figure D.16 True map (a) and clustering result (b) based on selected *HbT* features for ADHD-Migraine discrimination

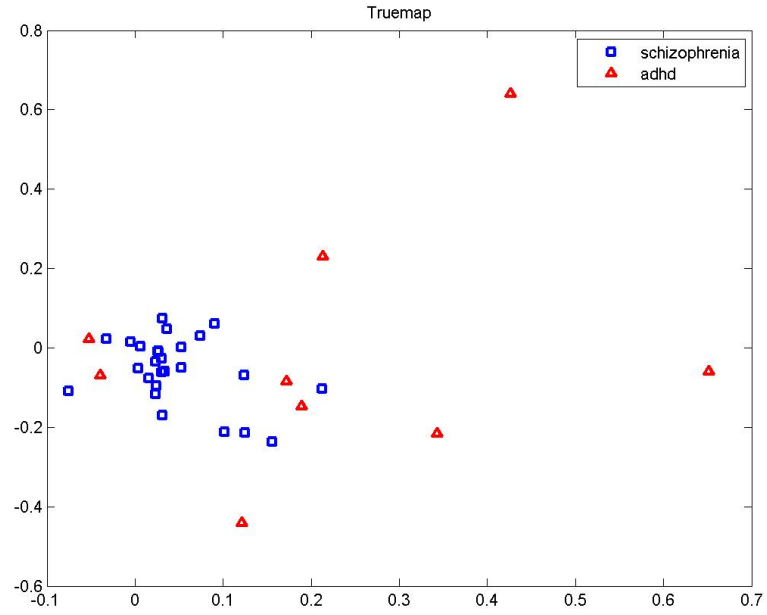


(a)

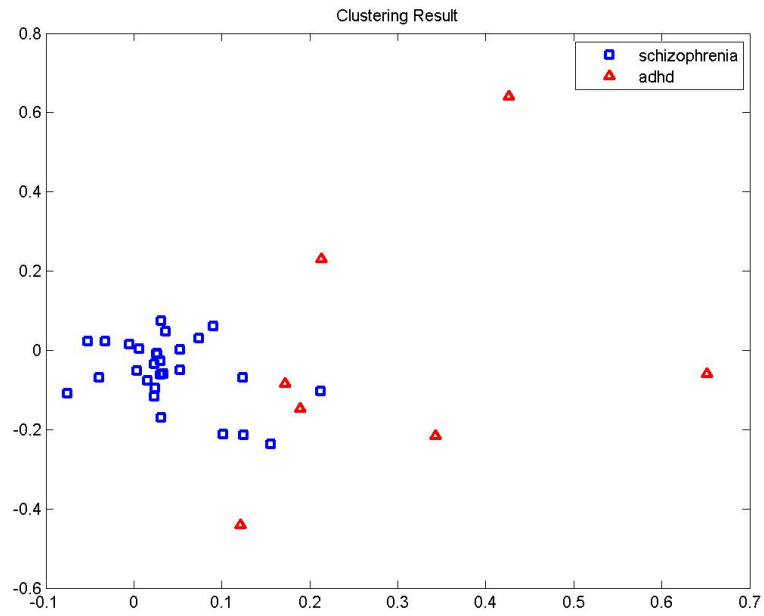


(b)

Figure D.17 Channel distribution (a) and frequency band distribution (b) of selected HbO_2 features for ADHD-Schizophrenia discrimination

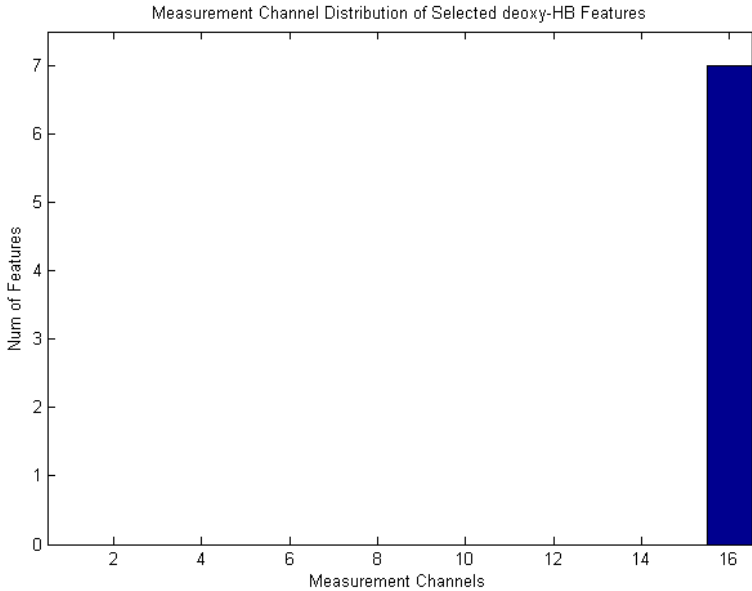


(a)

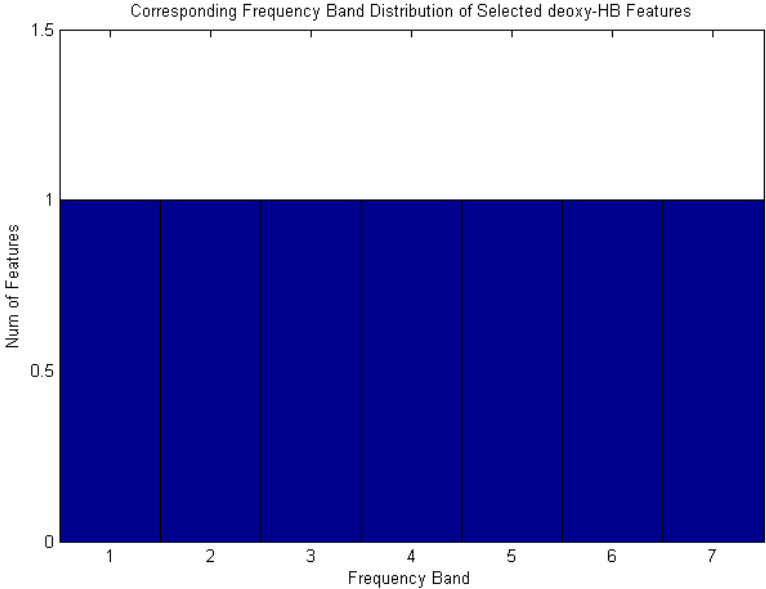


(b)

Figure D.18 True map (a) and clustering result (b) based on selected HbO_2 features for ADHD-Schizophrenia discrimination

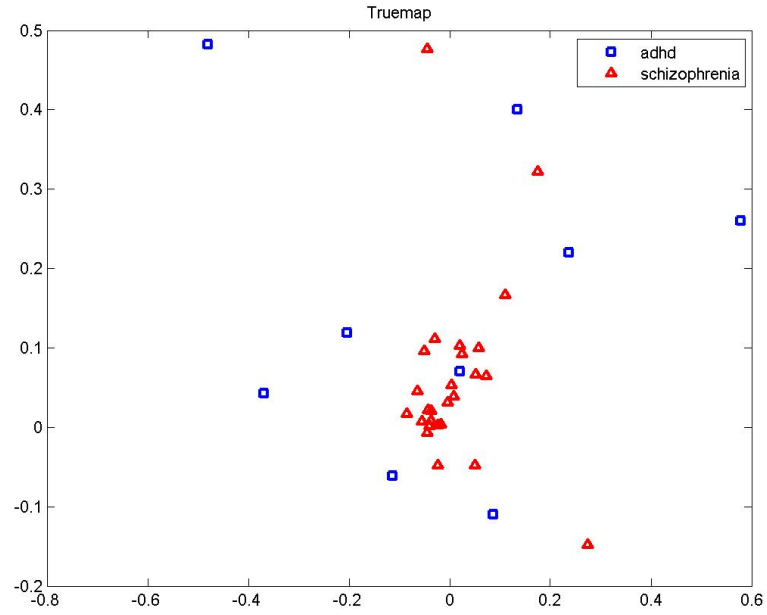


(a)

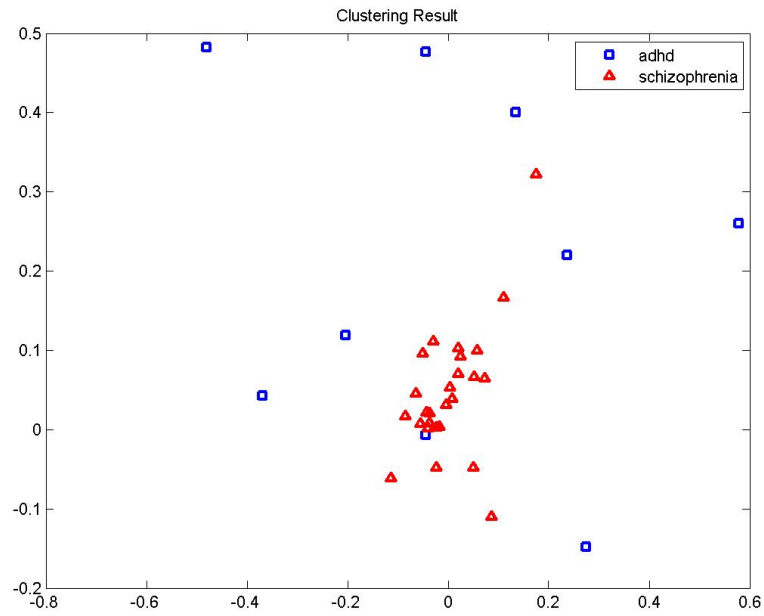


(b)

Figure D.19 Channel distribution (a) and frequency band distribution (b) of selected *Hb* features for ADHD-Schizophrenia discrimination

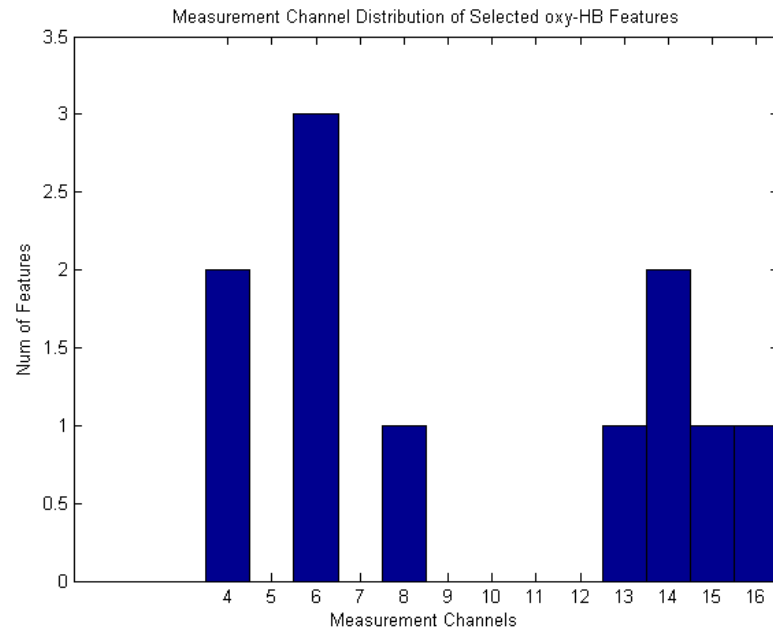


(a)

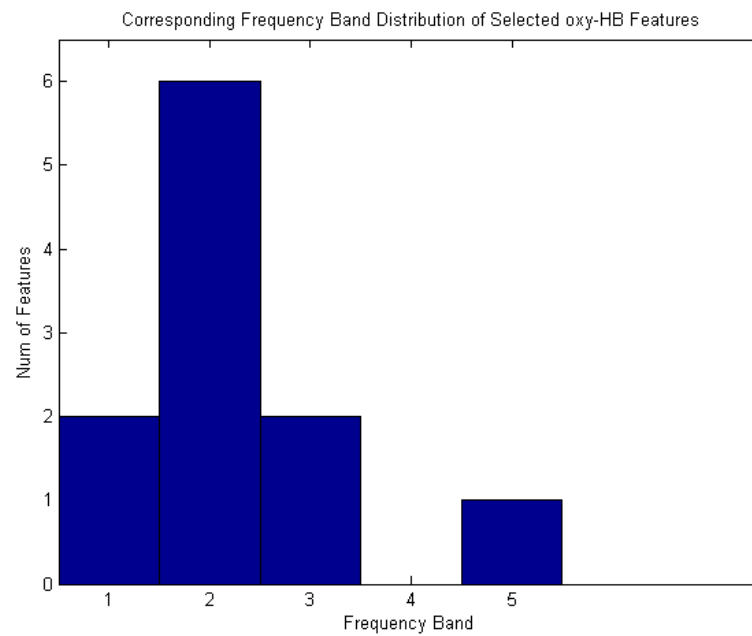


(b)

Figure D.20 True map (a) and clustering result (b) based on selected *Hb* features for ADHD-Schizophrenia discrimination

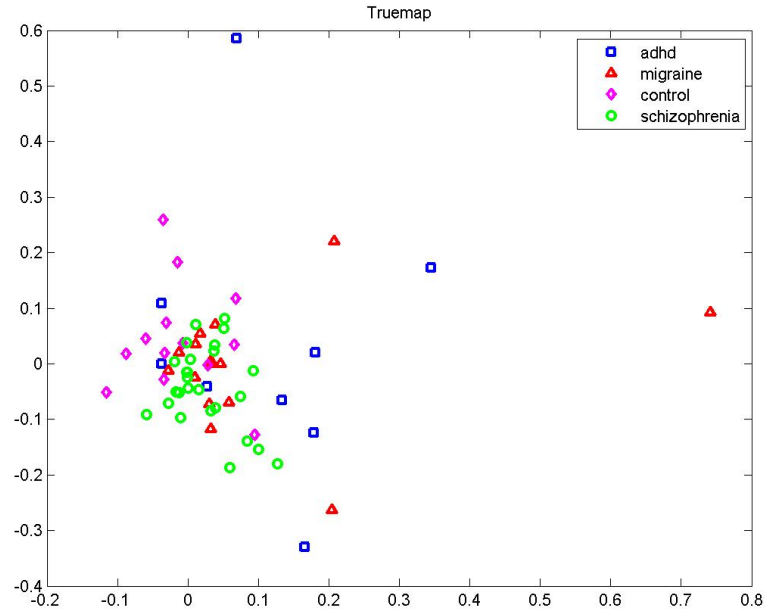


(a)

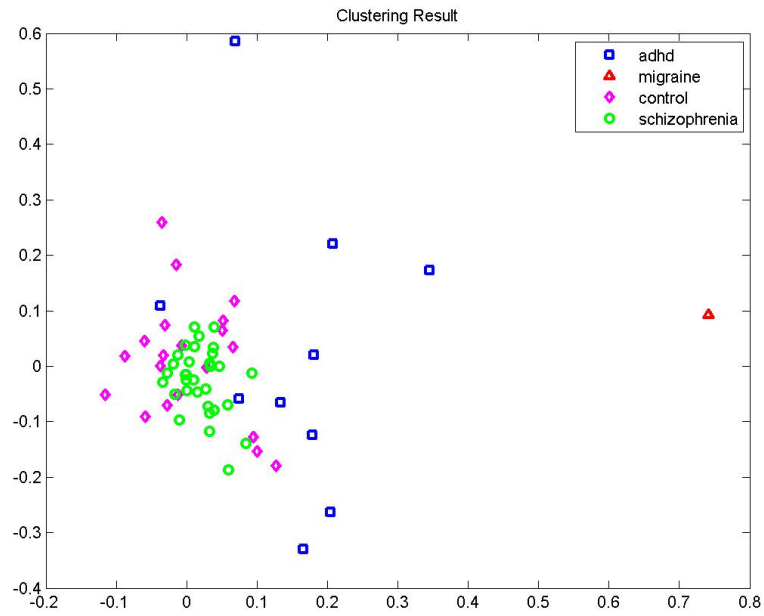


(b)

Figure D.21 Channel distribution (a) and frequency band distribution (b) of selected HbO_2 features for discrimination of all groups

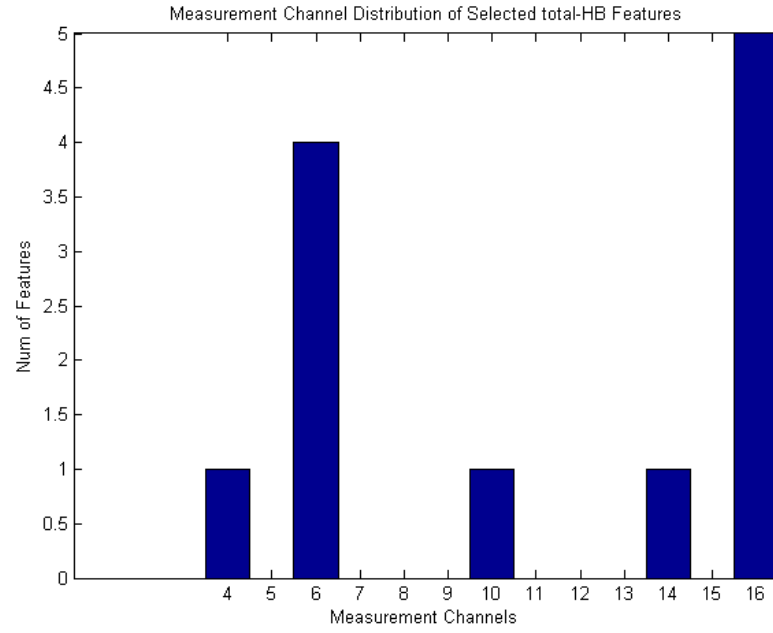


(a)

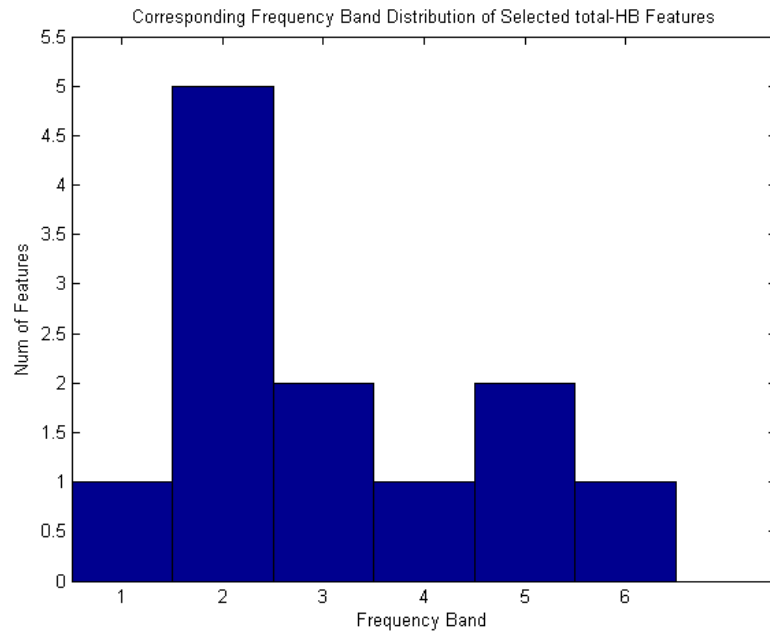


(b)

Figure D.22 True map (a) and clustering result (b) based on selected HbO_2 features for discrimination of all groups

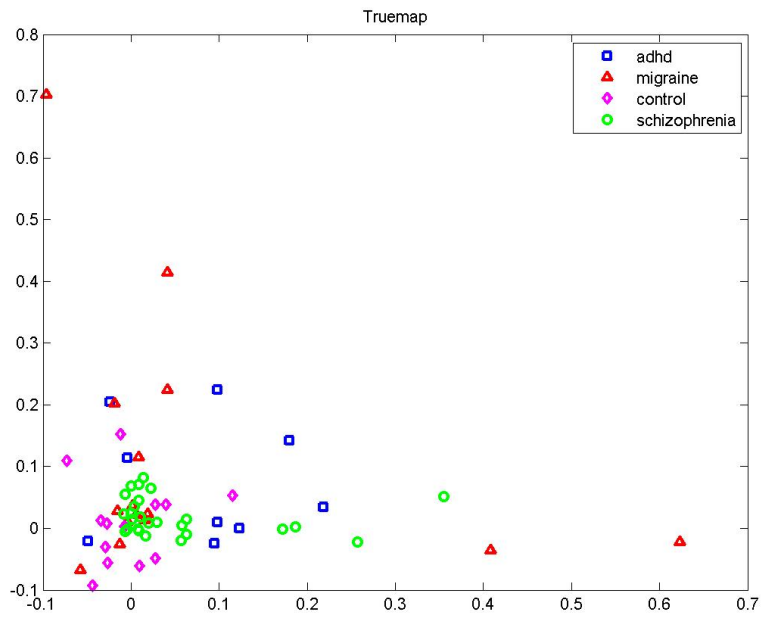


(a)

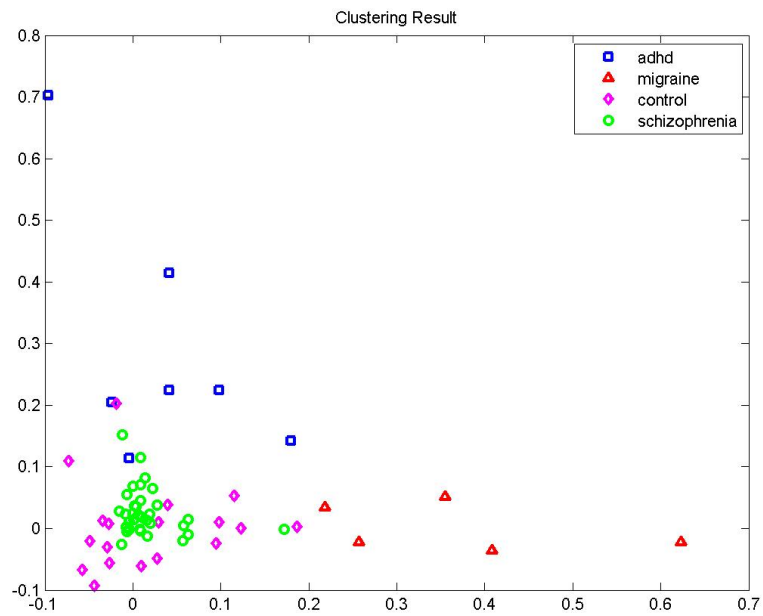


(b)

Figure D.23 Channel distribution (a) and frequency band distribution (b) of selected *HbT* features for discrimination of all groups



(a)



(b)

Figure D.24 True map (a) and clustering result (b) based on selected *HbT* features for discrimination of all groups

REFERENCES

1. Zysset, S., K. Muller, G. Lohmann, and D. Y. von Cramon, "Color-word matching stroop task: separating interference and response conflict," *Neuroimage*, no. 13, pp. 29–36, 2001.
2. Bunce, S. C., "Functional optical brain imaging using near-infrared during cognitive tasks," *International Journal of Human - Computer Interaction*, pp. 211–227, 2004.
3. Bunce, S. C., "Functional brain imaging using near-infrared technology," *IEEE Engineering in Medicine and Biology Magazine*, pp. 38–46, July/August 2007.
4. Negoro, H., M. Sawada, J. Iida, T. Ota, S. Tanaka, and T. Kishimoto, "Prefrontal dysfunction in attention-deficit/hyperactivity disorder as measured by near-infrared spectroscopy," *Child Psychiatry & Human Development*, Vol. 41, pp. 139–203, 2010.
5. Azechi, M., K. Ikezawa, H. Takahashi, L. Canuet, R. Kurimoto, T. Nakahachi, R. Ishii, M. Fukumoto, K. Ohi, Y. Yasuda, H. Kazui, and M. Takeda, "Discriminant analysis in schizophrenia and healthy subjects using prefrontal activation during frontal lobe tasks: A near-infrared spectroscopy," *Schizophrenia Research*, Vol. 117, pp. 52–60, 2010.
6. Ehlis, A. C., C. G. Bahne, C. P. Jacob, M. J. Herrmann, and A. J. Fallgatter, "Reduced lateral prefrontal activation in adult patients with attention-deficit/hyperactivity disorder (adhd) during a working memory task: A functional near-infrared spectroscopy (fnirs) study," *Journal of Psychiatric Research*, Vol. 42, pp. 1060–1067, November 2008.
7. Liboni, W., F. Molinari, G. Allais, O. Mana, E. Negri, G. Grippi, C. Benedetto, G. D'Andrea, and G. Bussone, "Why do we need nirs in migraine?," *Neurological Sciences: Official Journal of the Italian Neurological Society and of the Italian Society of Clinical Neurophysiology*, Vol. 28, pp. 222–224, 2007.
8. Akin, A., D. Bilensoy, U. E. Emir, M. Gulsoy, S. Candansayar, and H. Bolay, "Cerebrovascular dynamics in patients with migraine: near-infrared spectroscopy study," *Neuroscience Letters*, no. 400, pp. 86–91, 2006.
9. Calandre, E., J. Bembibre, M. Arnedo, and D. Becerra, "Cognitive disturbances and regional cerebral blood flow abnormalities in migraine patients: their relationship with the clinical manifestations of the illness," *Cephalalgia*, Vol. 22, pp. 291–302, 2002.
10. Backer, M., D. Sander, M. Hammes, D. Funke, M. Deppe, B. Conrad, and T. Tolle, "Altered cerebrovascular response pattern in interictal migraine during visual stimulation," *Cephalalgia*, Vol. 21, pp. 611–616, 2001.
11. Callicot, J. H., A. Bertolino, V. S. Mattay, F. J. P. Langheim, J. Duyn, R. Coppola, T. E. Goldberg, and D. R. Weinberger, "Physiological dysfunction of the dorsolateral prefrontal cortex in schizophrenia revisited," *Cerebral Cortex*, Vol. 10, pp. 1078–1092, November 2000.
12. Schytz, H. W., K. Ciftçi, A. Akin, M. Ashina, and H. Bolay, "Intact neurovascular coupling during executive function in migraine without aura: interictal near-infrared spectroscopy study," *Cephalalgia*, Vol. 30, pp. 457–466, Apr 2010.
13. Dora, B., and S. Balkan, "Exaggerated interictal cerebrovascular reactivity but normal blood flow velocities in migraine without aura," *Cephalalgia*, Vol. 22, pp. 288–290, 2002.

14. Facco, E., M. Munari, F. Baratto, A. Behr, A. D. Palu, S. Cesaro, M. Giacomini, and G. Giron, "Regional cerebral blood flow (rcbf) in migraine during the interictal period: different rcbf patterns in patients with and without aura," *Cephalalgia*, Vol. 16, pp. 161–168, 1996.
15. Heckmann, J., M. Hilz, A. Katalinic, H. Marthol, M. M.-W. M, and B. Neundorfer, "Myogenic cerebrovascular autoregulation in migraine measured by stress transcranial doppler sonography," *Cephalalgia*, Vol. 18, pp. 133–137, 1998.
16. Akin, A., and D. Bilensoy, "Cerebrovascular reactivity to hypercapnia in migraine patients measured with near-infrared spectroscopy," *Brain Research*, no. 1107, pp. 206–214, 2006.
17. Carter, C. S., W. Perlstein, R. Ganguli, J. Brar, M. Mintun, and J. D. Cohen, "Functional hypofrontality and working memory dysfunction in schizophrenia," *The American Journal of Psychiatry*, Vol. 155, pp. 1285–1287, 1998.
18. Curtis, V. A., E. T. Bullmore, M. J. Brammer, I. C. Wright, S. C. Williams, R. G. Morris, T. S. Sharma, and R. M. M. P. K. McGuire, "Attenuated frontal activation during a verbal fluency task in patients with schizophrenia," *The American Journal of Psychiatry*, Vol. 155, pp. 1056–1063, 1998.
19. Taniguchi, K., S. Sumitani, Y. Watanabe, M. Akiyama, and T. Ohmori, "Multi-channel near-infrared spectroscopy reveals reduced prefrontal activation in schizophrenia patients during performance of the kana stroop task," *The Journal of Medical Investigation*, Vol. 59, pp. 45–52, February 2012.
20. Quaresima, V., P. Giosue, R. Roncone, M. casacchia, and M. Ferrari, "Prefrontal cortex dysfunction during cognitive tests evidenced by functional near-infrared spectroscopy," *Psychiatry Research: Neuroimaging*, Vol. 171, pp. 252–257, 2009.
21. Wender, P. H., "Attention-deficit hyperactivity disorder in adults," *The Psychiatric clinics of North America*, Vol. 21, pp. 761–774, 1998.
22. Yasumura, A., N. Kokubo, H. Yamamoto, Y. Yasumura, E. nakagawa, M. Kaga, K. Hiraki, and M. Inagaki, "Neurobehavioral and hemodynamic evaluation of stroop and reverse stroop interference in children with attention-deficit/hyperactivity disorder," *Brain & Development*, July/August 2013.
23. Xiao, T., Z. Xiao, X. Ke, S. Hong, H. Yang, Y. Su, K. Chu, X. Xiao, J. Shen, and Y. Liu, "Response inhibition impairment in high functioning autism and attention deficit hyperactivity disorder: Evidence from near-infrared spectroscopy data," *Plos One*, Vol. 7, October 2012.
24. Pereira, F., T. Mitchell, and M. Botvinick, "Machine learning classifiers and fmri: a tutorial overview," tech. rep., Carnegie Mellon University, Pittsburgh PA 15213, July 2008.
25. Formisano, E., F. D. Martino, and G. Valente, "Multivariate analysis of fmri time series: Classification and regression of brain responses using machine learning," in *Magnetic Resonance Imaging*, pp. 921–934, 2008.
26. Escudero, J., R. Hornero, D. Abasalo, and A. Fernandez, "Comparison of blind source separation preprocessing applied magnetoencephalogram recordings to improve the classification of alzheimer's diseases patients," *International Journal of Bioelectromagnetism*, Vol. 12, no. 4, pp. 183–189, 2010.

27. Lopez, M., J. Ramirez, J. M. Gorriz, D. Salas-Gonzalez, I. Alvarez, F. Segovia, and C. G. Puntonet, "Automatic tool for alzheimer's disease diagnosis using pca and bayesian classification rules," *IEEE Xplore*, Vol. 45, April 2009.
28. Delpy, D. T., and M. Cope, "Quantification in tissue near-infrared spectroscopy," *Philosophical Transactions of the Royal Society of London. Series B*, Vol. 352, pp. 649–659, 1997.
29. Sayli, O., E. B. Aksel, and A. Akin, "Crosstalk and error analysis of fat layer on continuous wave near-infrared spectroscopy measurements," *Journal of Biomedical Optics*, Vol. 13, November/December 2008.
30. Sayita, Y., "Classification of migraineurs using functional near infrared spectroscopy data," Master's thesis, The Graduate School of Informatics of The Middle East Technical University, Ankara, Turkey, 2012.
31. Boas, D. A., A. M. Dale, and M. A. Franceschini, "Diffuse optical imaging of brain activation: Approaches to optimizing image sensitivity, resolution, and accuracy," *NeuroImage* 23, pp. 275–288, 2004.
32. Wilcox, T., H. Bortfeld, R. Woods, E. Wruck, and D. A. Boas, "Using near-infrared spectroscopy to assess neural activation during object processing in infants," *Journal of Biomedical Optics*, 2005.
33. Sweeney, K. T., H. Ayaz, T. E. Ward, M. Izzetoglu, S. F. McLoone, and B. Onaral, "A methodology for validating artifact removal techniques for physiological signals," *IEEE Transactions on Information Technology in Biomedicine*, Vol. 16, September 2012.
34. Virtanen, J., T. Noponen, and P. Merilainen, "Comparison of principal and independent component analysis in removing extracerebral interference from near-infrared spectroscopy signals," *Journal of Biomedical Optics*, Vol. 14, September /October 2009.
35. Scholkmann, F., S. Spichtig, T. Muehlemann, and M. Wolf, "How to detect and reduce movement artifacts in near-infrared imaging using moving standard deviation and spline interpolation," *Physiological Measurement*, Vol. 31, pp. 649–662, March 2010.
36. Hyvarinen, A., J. Karhunen, and E. Oja, *Independent Component Analysis*, A Wiley-Interscience Publication, 2001.
37. Mingoti, S. A., and J. O. Lima, "Comparing som neural network with fuzzy c-means, k-means and traditional hierarchical clustering algorithms," *European Journal of Operational Research*, Vol. 174, pp. 1742–1759, July/August 2006.
38. Kovacs, F., C. Legany, and A. Babos, "Cluster validity measurement techniques," tech. rep., Department of Automation and Applied Informatics, Budapest University of Technology and Economics, Goldmann Gyorgy ter 3, H-1111 Budapest, Hungary.
39. Robertson, F. C., T. S. Douglas, and E. M. Meintjes, "Motion artifact removal for functional near infrared spectroscopy: A comparison of methods," *IEEE Transactions on Biomedical Engineering*, Vol. 57, pp. 1377–1387, June 2010.
40. Rummel, C., R. K. Verma, V. Schopf, E. Abela, M. Hauf, J. F. Z. Berruecos, and R. Wiest, "Time course based artifact identification for independent components of resting-state fmri," *frontiers in Human Neuroscience*, Vol. 7, May 2013.

41. Lu, Q., H. Jiang, G. Luo, Y. Han, and Z. Yao, "Multichannel matching pursuit of meg signals for discriminative oscillation pattern detection in depression," *International Journal of Psychophysiology*, Vol. 88, pp. 206–212, 2013.
42. Storti, S. F., E. Formaggio, R. Nordio, P. Manganotti, A. Fiaschi, A. Bertoldo, and G. M. Toffolo, "Automatic selection of resting-state networks with functional magnetic resonance imaging," *frontiers in Neuroscience*, Vol. 7, May 2013.
43. Bezdek, J. C., R. Ehrlich, and W. Full, "Fcm: The fuzzy c-means clustering algorithm," *Computers & Geosciences*, Vol. 10, no. 2–3, pp. 191–203, 1984.